ALGERIAN DEMOCRATIC AND POPULAR REPUBLIC

MINISTRY OF HIGHER EDUCATION AND SCIENTIFIC RESEARCH

Mohamed El-Bachir El-Ibrahimi University - Bordj Bou Arreridj

Faculty of Science and Technology

Department of Electronics

Master's Thesis

Presented to obtain

MASTER'S DEGREE

FIELD: ELECTRONICS

Specialization: Microelectronics

By

Madani Mohammed Younes

Title

Study of the Physical Properties of the Ordered SiSn Alloy in the Cubic Zinc-blende Phase

Defended on: 11/06/2025

Name & Surname	Grade	Role	Institution
M me . Fadila KHERRAT	*MAA*	*President*	*Univ-BBA*
Mme. Nadhira BIOUD	*MCA*	*Supervisor*	*Univ-BBA*
Mr. Abdelfateh BENMAKHLOUF	*MCB*	*Co-Supervisor*	*Univ-BBA*
M r . Abdelouahab DJEMOUAI	*MCB*	*Examiner*	*Univ-BBA*

Academic Year 2024/2025

Acknowledgments

Dedication

I dedicate this work, a symbol of effort and perseverance:

To my dear mother and father,

For their unconditional love, unwavering support, and countless sacrifices that have allowed me to reach this point. Their trust in me has always been a source of motivation and strength.

To my brothers, Iyad and Abdelhaq,

For their invaluable presence, encouragement, and support throughout this journey.

To my friends AbdSamed, Anis, Bilal, Younes, Yehya, and Mouath,

For their true friendship, unwavering support, and all the moments we shared that made this journey more enjoyable and enriching.

To my professors,

For their guidance, dedication, and the valuable knowledge they have imparted to me, helping me grow both academically and personally.

To all those who have believed in me and supported me, near or far,

This achievement is also yours.

Table of Contents

Chapter 2: Theoretical Approaches Using First-Principles Calculations

Chapter 3: Calculation Method, Results Presentation, and Their Discussion

Table of Tables

I

Table of Figures

List of Abbreviations

Abbreviation	Meaning
Si	Silicon
Sn	Tin
SiSn	Silicon-Tin alloy
DFT	Density Functional Theory
LDA	Local Density Approximation
GGA	Generalized Gradient Approximation
DOS	Density of States
FFT	Fast Fourier Transform
SCF	Self-Consistent Field
CBM	Conduction Band Minimum
VBM	Valence Band Maximum
FCC	Face-Centered Cubic
CASTEP	Cambridge Serial Total Energy Package
MOCVD	Metal Organic Chemical Vapor Deposition
MBE	Molecular Beam Epitaxy
TCO	Transparent Conductive Oxide
PBE	Perdew-Burke-Ernzerhof (exchange-correlation functional)
II-VI	Group II-VI semiconductors
III-V	Group III-V semiconductors
IV-IV	Group IV-IV semiconductors
E-V	Energy-Volume
P-V	Pressure-Volume
BSE	Bethe-Salpeter Equation

List of Symbols

Symbol	Meaning
a_0	Lattice constant at equilibrium
P	Pressure
$E(V)$	Total energy as a function of volume
V_0	Equilibrium volume
B_0	Bulk modulus
B_0'	Pressure derivative of the bulk modulus
g	Theoretical mass density
$\hbar\omega$	Photon energy
$\varepsilon(\omega)$	Dielectric function (complex)
$\varepsilon_1(\omega)$	Real part of dielectric function
$\varepsilon_2(\omega)$	Imaginary part of dielectric function
$\alpha(\omega)$	Optical absorption coefficient
$\sigma(\omega)$	Optical conductivity
$L(\omega)$	Electron energy loss function
$n(\omega)$	Refractive index
$R(\omega)$	Optical reflectivity
Ecut	Cut-off energy
nkpt	Number of k-points for Brillouin zone sampling
Eg	Energy band gap
NA	Avogadro's number
M	Molar mass
k	Wave vector
ψ	Wave function
$\rho(r)$	Electron density at position r

General Introduction

General Introduction

The new era of semiconductor technology increasingly seeks its raw materials from the periodic table of elements, relying on the natural principle that the combination of two or more different elements does not simply merge their individual properties but instead gives rise to new characteristics. This principle has led to the development of entire families of alloys, such as III–V, II–VI, and I–VII compounds, whose potential applications continue to be explored [1].

However, the experimental realisation of new materials often poses significant challenges due to the complexity and high cost involved. These difficulties have driven researchers to seek alternative approaches. Thanks to the tremendous advances in computational tools, numerical simulation has become an indispensable complement to experimentation, providing predictive data that can guide and validate experimental studies.

Several simulation methods have been developed for the predictive calculation of the structural, electronic, and optical properties of complex systems. Among these, first-principles (ab initio) methods have proven particularly powerful. In the present work, we adopt such an approach using the CASTEP simulation code.

This thesis aims to contribute to the study of the structural, electronic, and optical properties of the binary SiSn alloy in the cubic zinc-blende phase.

The manuscript is organised into three chapters, along with a general introduction and a general conclusion. The first chapter presents an overview of semiconducting materials, summarising their fundamental properties. The second chapter outlines the theoretical foundations, including the key approximations, Density Functional Theory (DFT) and some other computational techniques employed. The third chapter is devoted to the presentation and discussion of the results obtained from our simulations concerning the characterisation of the cubic zinc-blende SiSn alloy.

The thesis concludes with a general conclusion summarising the main findings and perspectives for future work.

Chapter I:
General information on semiconductors

I.1 Introduction

Semiconductors are a class of materials whose electrical conductivity lies between that of conductors and that of insulators, making them indispensable in modern electronic and optoelectronic applications. Unlike metals, where electrons move freely due to the presence of a partially filled conduction band, semiconductors have a well-defined band gap - an energy range in which electronic states do not exist. This band gap, which separates the valence band (where electrons are bound to atoms) from the conduction band (where electrons can move freely and contribute to electrical conduction), determines the electrical behaviour of semiconductor materials. The ability to control the carrier concentration through doping, and the dependence of their electrical properties on external stimuli such as temperature, pressure and illumination, make semiconductors a cornerstone of modern technology. They play a vital role in a wide range of applications including microelectronics, optoelectronic devices (e.g. LEDs, lasers and photodetectors) and energy conversion technologies such as solar cells and thermoelectric generators [1].

Silicon (Si) has long remained the dominant material in semiconductor technology, largely due to its natural abundance, chemical stability, and the maturity of processing methods like photolithography and chemical vapour deposition. Despite these advantages, there has been growing interest in alternative materials that offer more adaptable electronic properties. In particular, compound semiconductors have attracted attention because they allow greater control over key characteristics such as band structure, carrier mobility, and optical response. These materials are often grouped according to the types of elements they contain — including III–V compounds like gallium arsenide (GaAs) and indium phosphide (InP), II–VI materials such as zinc sulphide (ZnS) and cadmium telluride (CdTe), and IV–IV systems like silicon–germanium (SiGe) and silicon–tin (SiSn). What makes these materials especially promising is their versatility: they can support applications ranging from high-speed electronics and infrared detection to quantum well devices and next-generation solar cells. Moreover, modern fabrication techniques, including molecular beam epitaxy and metal-organic chemical vapour deposition (MOCVD), enable precise control at the atomic level, which is essential for tuning their properties to suit specific device requirements [2].

1.2 Classification of semiconductors

Semiconductors can be classified on the basis of their composition, electrical properties and the mechanisms that control their charge transport. The two main categories of semiconductors are

intrinsic and extrinsic, with the latter further subdivided into n-type and p-type depending on the nature of the dopants introduced.

I.2.1 Intrinsic semiconductors

Intrinsic semiconductors are pure materials whose electrical behaviour is determined entirely by their atomic structure, without the influence of added impurities. Silicon (Si) and germanium (Ge) are the most well-known examples, both forming a diamond cubic crystal lattice. In these materials, electrical conductivity arises when electrons gain enough thermal energy to move from the valence band into the conduction band, leaving behind holes. These electron-hole pairs enable charge transport within the crystal [3].

The number of free carriers in an intrinsic semiconductor is strongly influenced by temperature. As thermal energy increases, more electrons are excited across the band gap, causing the intrinsic carrier concentration n_i to rise exponentially. A key factor in this process is the band gap energy Eg , which defines how easily electrons can be excited. For instance, silicon has a band gap of around 1.12 eV at room temperature, while germanium's narrower gap of 0.66 eV allows it to conduct more effectively at lower temperatures [4].

While intrinsic semiconductors are essential for building a solid understanding of semiconductor physics, their low carrier concentration under normal conditions limits their use in practical devices. As a result, most applications rely on doping these materials to enhance their conductivity and fine-tune their electronic properties [4].

I.2.2 Extrinsic semiconductors (doped semiconductors)

To improve conductivity and control carrier concentration, intrinsic semiconductors are deliberately doped with small amounts of impurity atoms. This process introduces additional free charge carriers - either electrons or holes - creating extrinsic semiconductors. Depending on the type of dopant introduced, extrinsic semiconductors are classified as either n-type or p-type [4].

I.2.2.1 n-type semiconductors

An n-type semiconductor is created by introducing Group V elements such as phosphorus (P), arsenic (As), or antimony (Sb) into a pure silicon lattice. These dopants have five valence electrons, one more than silicon's four. When substituted into the crystal structure, the extra electron is only loosely bound to the atom and can be easily excited into the conduction band.

This results in a significant increase in free electrons, which become the dominant charge carriers in n-type materials [4].

The presence of these additional electrons enhances the electrical conductivity of the material. In n-type semiconductors, the Fermi level moves closer to the conduction band, indicating a greater likelihood of electron occupation at higher energy states. This shift is a direct consequence of the elevated electron concentration, n-type doping is a fundamental process in semiconductor fabrication, particularly in the production of devices like transistors, where efficient electron transport is essential for performance and speed.

I.2.2.2 p-type semiconductors

A p-type semiconductor is produced by adding Group III elements such as boron (B), aluminium (Al), or gallium (Ga) to an intrinsic semiconductor like silicon. These dopants each have three valence electrons, which is one fewer than silicon's four. As a result, when they are introduced into the silicon crystal lattice, they generate electron deficiencies known as "holes" in the valence band. These holes behave like positive charge carriers: they allow surrounding electrons to shift into the vacant positions, which in turn facilitates charge movement and increases the material's overall conductivity [4].

In this type of material, the Fermi level shifts closer to the valence band, reflecting the higher hole concentration. This shift is especially important in semiconductor junctions. At p–n junctions, for instance, holes from the p-type side recombine with electrons from the n-type side, allowing for essential functions like current rectification and signal modulation [1].

The process of doping is a cornerstone of semiconductor engineering. By carefully introducing donor or acceptor atoms, engineers can fine-tune the electrical characteristics of a material to meet specific device requirements. The interaction between p-type and n-type regions underpins the operation of key components such as diodes, transistors, and integrated circuits technologies that serve as the foundation of modern electronic systems [1, 5].

Figure **I.1** shows a comparison of p-type and n-type semiconductors [6].
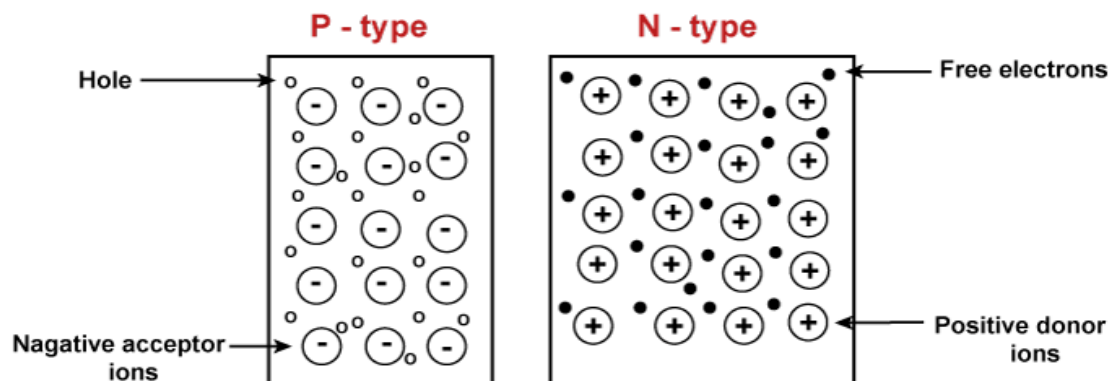
Figure I.1: Comparison of p-type and n-type semiconductors [6].

I.3 Classification of compound semiconductors

In contrast to elemental semiconductors such as silicon (Si) and germanium (Ge), compound semiconductors are composed of two or more elements, typically from different groups of the periodic table. These materials often exhibit superior optoelectronic properties, including tunable band gaps, higher carrier mobility and strong optical absorption, making them essential for high-speed electronics, optoelectronic devices and energy applications [7, 8].

Compound semiconductors can be further classified based on their composition:

- Binary semiconductors: Consist of two elements.

- Ternary semiconductors: Contain three elements, offering greater flexibility in band gap tuning.

- Quaternary semiconductors: Incorporate four elements, allowing even more precise control of electronic and optical properties.

Table I.1 Classification of different types of semiconducting materials [9].

Compounds	Types of semiconductor	Examples
Binary	II–VI compound	ZnS, ZnSe, ZnTe, CdS, CdSe, etc.
	III–V compound	AlAs, GaN, GaAs, InP, InAs, InSb, etc.
	IV–IV compound	SiC, SiGe, etc.
Ternary		GaAsP, HgCdTe, AlGaAs, etc.
Quaternary		InGaAsP

The following table provides an overview of different types of compound semiconductors along with their representative materials:

III-V Semiconductors

III-V semiconductors are composed of group III (e.g. Ga, In, Al) and group V (e.g. As, P, N, Sb) elements. They are widely used in high-speed electronics, light-emitting diodes (LEDs) and laser diodes due to their direct band gaps, which allow efficient radiative recombination [7, 8].

Common III-V semiconductors include:

- Gallium arsenide (GaAs)**:** Used in high-frequency transistors, photodetectors, and optoelectronic devices.

- Indium phosphide (InP)**:** widely used for fiber-optic communications and high-speed electronic applications.

- Gallium nitride (GaN)**:** A key material for power electronics, blue LEDs, and high-temperature applications.

The direct band gap property of these materials makes them particularly valuable for photonic applications such as semiconductor lasers and solar cells (Table 1.1) [5].

II-VI semiconductors

II-VI semiconductors consist of elements from group II (e.g. Zn, Cd) and group VI (e.g. S, Se, Te). These materials are known for their strong optical absorption, making them highly suitable for solar cells, photodetectors and quantum dot technologies [7].

Exemples include :

- Zinc sulfide (ZnS): Used in electroluminescent displays and UV photodetectors.
- Cadmium telluride (CdTe): One of the leading materials for thin-film solar cells, offering an optimal band gap for photovoltaic applications.
- Zinc oxide (ZnO): A transparent conducting oxide widely employed in opto-electronic devices and gas sensors.

Due to their high absorption coefficients, II-VI semiconductors are integral to photonic and photovoltaic applications, enabling efficient light conversion and emission (Table 1.1).

IV-IV semiconductors

IV-IV semiconductors consist of Group IV elements such as silicon (Si), germanium (Ge) and tin (Sn). These materials are particularly attractive due to their compatibility with Si-based semiconductor technology, allowing seamless integration into existing electronic manufacturing processes [10].

Notable IV-IV semiconductors include:

- Silicon-germanium (SiGe)**:** Used in high-speed transistors, strain engineering, and heterojunction bipolar transistors (HBTs). By incorporating Ge, the material exhibits enhanced carrier mobility and tunable band gaps.

- Silicon-tin (SiSn)**:** A promising semiconductor for optoelectronic applications**,** offering band gap tunability that can be leveraged for near-infrared photonic devices and strain-enhanced electronic performance.

These materials are increasingly relevant inadvanced CMOS technology, where they provide enhanced device performance and enable novel functionalities in next-generation semiconductor devices (Table 1.1) [5, 10].

I.4 Electronic properties of semiconductors

The electronic properties of semiconductors are primarily determined by their energy band structure, which determines their electrical and optical behaviour. Understanding these properties is crucial for the design of semiconductor-based devices such as transistors, diodes and optoelectronic components.

I.4.1 Energy band structure

The energy band structure of a material determines whether it functions as a conductor, semiconductor or insulator, based on the presence and width of the band gap (E_g):

- Conductors (e.g. metals): Have no band gap ((E_g= 0), allowing free movement of electrons within the conduction band, resulting in high electrical conductivity.

- Semiconductors (e.g. Si, GaAs): Have a moderate band gap (0.6 - 3.5 eV), which allows controlled electrical conductivity. At room temperature, some electrons gain enough energy to jump from the valence band to the conduction band.

- Insulators (e.g. diamond): Have a large band gap ($E_g > 5$ eV), which prevents electrons from easily moving to the conduction band, making them poor electrical conductors [4]

I.4.2 Direct vs. indirect band gap semiconductors

Semiconductors can be further classified based on the relationship between the conduction band minimum (CBM) and the valence band maximum (VBM) in momentum space.

1.4.2.1 Direct band gap semiconductors

In direct band gap semiconductors (Figure **1.2 a**), the CBM and VBM occur at the same momentum (k-space position), enabling electrons to transition between these bands without requiring phonon assistance. This results in efficient photon emission, making these materials ideal for:

- Light-emitting diodes (LEDs)

- Laser diodes

- Photovoltaiccells (solarcells)

Examples: Gallium arsenide (GaAs), Cadmium telluride (CdTe), and Indium phosphide (InP) exhibit direct band gaps, making them highly efficient for optoelectronic applications [11].

I.4.2.2 Indirect band gap semiconductors:

In indirect bandgap semiconductors (**Figure 1.2 b**)*,* CBM and VBM occur with different momenta, meaning that electron transitions require an additional phonon to conserve momentum. This makes them less efficient for light emission, but highly suitable for electronic applications such as:

- Transistors and integrated circuits (ICs)

- Complementary metal-oxide-semiconductor (CMOS) technology

- Power electronics

Examples: Silicon (Si) and Germanium (Ge) are well-known indirect band gap semiconductors, widely used in microelectronics [4].
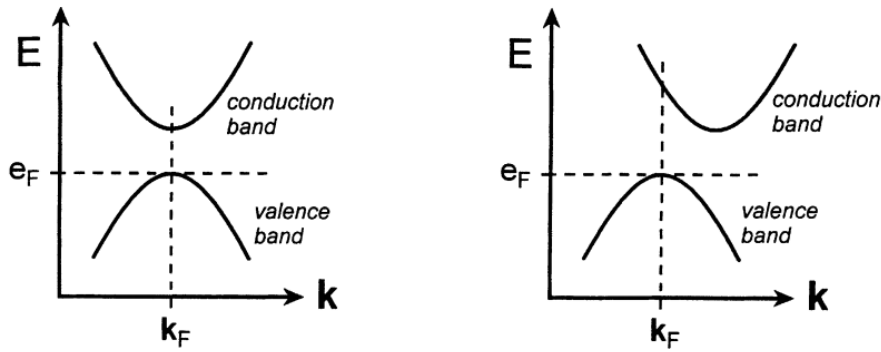
Figure I.2: (a) Direct gap semiconductor, (b) Indirect gap semiconductor [12].

I.4.3 Electronic band structure

In computational condensed matter physics, the energy dispersion relation is calculated along high-symmetry paths in the Brillouin zone to determine the band gap Eg. Exchange–correlation effects are addressed using suitable density functionals, such as the Generalised Gradient Approximation (GGA) or hybrid functionals, which enhance the accuracy of the computed band gap. **Figure I.3** presents an example of the band structure for the SiGe semiconductor material [13].
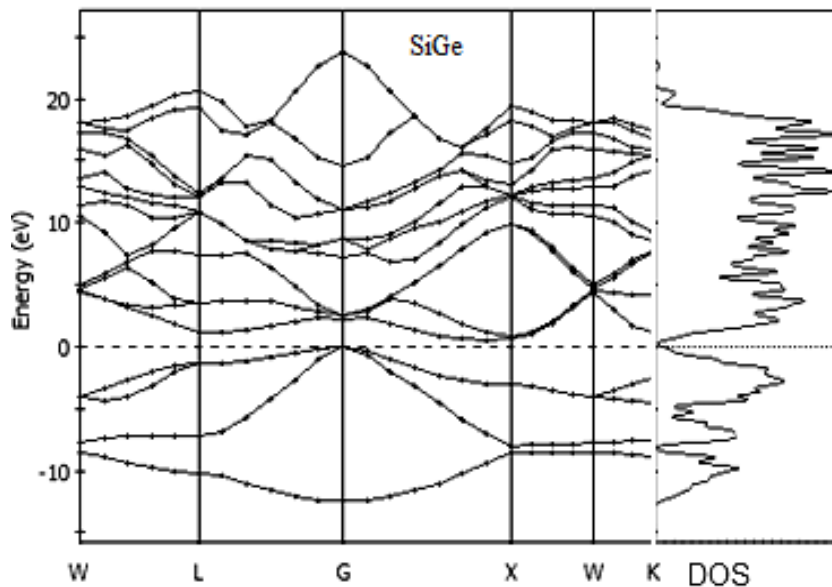
Figure I.3: Band structure of SiGe [13].

I.4.4 Optical properties

- The dielectric function $\epsilon(\omega)$ is computed using linear response theory [10], which accounts for the interaction between the material and electromagnetic radiation.

- Optical spectra, such as absorption and reflectivity, are derived from the

calculated dielectric function to evaluate the alloy's potential for optoelectronic applications.

These steps provide a comprehensive understanding of the structural, electronic, and optical properties of the SiSn alloy, offering valuable insights into its applications in semiconductor technology.

I.5 Optical properties of semiconductors

The optical properties of semiconductors describe their interaction with electromagnetic radiation, playing a crucial role in applications such as solar cells, LEDs, laser diodes, and photodetectors. These properties are intrinsically tied to a semiconductor's band structure, phonon interactions, and doping concentration, all of which influence light absorption and emission.

I.5.1 Key optical phenomena in semiconductors

1. **Refraction:**

   - When light enters a semiconductor, its speed changes due to the material's refractive index (n), causing the light to bend.

   - Governed by Snell's Law, refraction is critical for designing waveguides, optical fibers, and lens coatings in photonic devices [7].

2. **Absorption:**

   - If a photon's energy matches or exceeds the band gap energy (E_g), it excites an electron from the valence band to the conduction band.

   - Direct band gap semiconductors (e.g., GaAs, CdTe) show strong absorption, making them ideal for solar cells and photodetectors [14].

3. **Transmission:**

   - Not all light is absorbed; some passes through the material without significant interaction.

   - High transmission is desirable in transparent conductive oxides (TCOs), used in display panels and touchscreens [7].

4. **Reflectivity:**

- Some light is reflected at the surface, leading to optical losses in devices like solar cells and photodetectors.

- Anti-reflective coatings (ARCs) are applied to minimize reflection and maximize light absorption in photovoltaic modules [14].

These interactions are illustrated in **Figure I.4**, which shows how light behave upon striking a semiconductor surface.
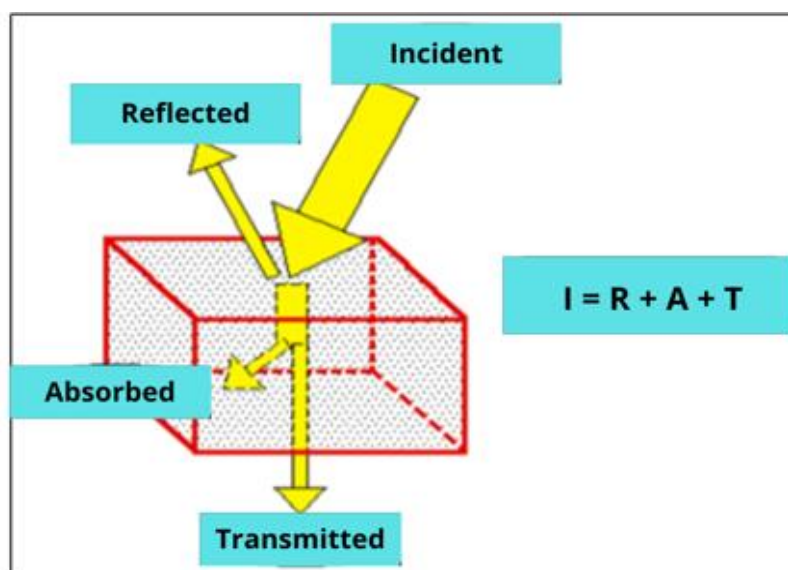
Figure. I.4: Different phenomena occurring during light-matter interaction [15].

I.6 First-principles calculations in semiconductor research

Understanding semiconductor properties requires both experimental and theoretical approaches. Among theoretical methods, first-principles (ab initio) calculations, particularly Density Functional Theory (DFT), have become indispensable for predicting and analyzing material properties at the atomic and electronic levels. These computational techniques eliminate the need for empirical parameters, providing highly accurate insights into the behavior of semiconductors under various conditions [16].

I.6.1 Key applications of first-principles methods

1. **Electronic band structures & density of states (DOS)**

- First-principles calculations provide a detailed picture of the electronic band structure, revealing information about band gaps, conduction and valence bands, and effective masses of charge carriers.

- The Density of States (DOS) function helps identify which electronic states are available at a given energy level, influencing electrical conductivity and optical absorption in semiconductors.

2. **Electronic& optical property predictions**

- DFT-based simulations enable the calculation of optical absorption spectra, dielectric functions, and refractive indices, which are crucial for designing solar cells, LEDs, and laser diodes.

- Advanced techniques such as GW approximation and Bethe-Salpeter Equation (BSE) refine band gap predictions, overcoming the underestimation issue in standard DFT calculations.

3. **Effects of pressure & strain engineering**

- Applying external pressure or strain modifies the electronic structure of semiconductors, leading to band gap tuning.

- This is particularly important for strain-engineered materials like SiGe and SiSn, which can be tailored for high-mobility transistors and optoelectronic applications.

4. **Electron-phonon interactions & carrier mobility**

- Charge carrier dynamics are influenced by electron-phonon interactions, which determine scattering rates, carrier lifetimes, and transport properties.

- First-principles methods help predict carrier mobility, a key factor in designing high-speed electronic and thermoelectric devices.

5. **Defect formation & interface engineering in semiconductor heterostructures**

- Semiconductor devices often contain defects and impurities that affect performance. First principles studies analyze:

  o Defect formation energies (stability of vacancies, interstitials, and substitutional defects).

  o Trap states and charge recombination centers, critical for optoelectronic device efficiency.

          ○   Interfacial properties in heterostructures, guiding the design of high-performance transistors and quantum devices.

6. **Exploring emerging 2D semiconductor materials**

- Beyond conventional semiconductors, DFT is widely used to study two-dimensional (2D) materials, such as:

   - Transition Metal Dichalcogenides (TMDs) (e.g., MoS2, WS_2), promising for flexible electronics and quantum devices.

   - Graphene and Silicene, with unique electronic properties for nanoscale transistors.

These materials hold potential for next-generation low-power electronics and photonic applications [17].

I.7 Effect of hydrostatic pressure [11]

It is well established that hydrostatic pressure has a significant influence on the electronic band structure of semiconductors. By compressing the lattice, pressure modifies the interatomic distances, thereby altering the electronic states and shifting the band gap energy.

I.7.1 Band gap evolution with pressure

The variation of the band gap with pressure can be described using an empirical equation [11]:

$$E_g(\text{P})=E_g(0)+\alpha\text{P}+\beta\text{P}^2 \tag{I.1}$$

where:

- $E_g(\text{P})$ is the band gap at pressure P,

- $E_g(0)$ is the band gap at ambient pressure,

- α and β are material-dependent coefficients that capture the linear and nonlinear pressure dependencies.

As shown in **Figure I.5**, which illustrates the band gap variation of 2L, 3L, and bulk SiSn under hydrostatic pressure [18], the band gap of the alloy exhibits notable changes as pressure increases. This pressure-induced modulation plays a key role in tailoring the electronic and optical properties of the material, offering promising potential for high-performance semiconductor and optoelectronic applications [8, 10].
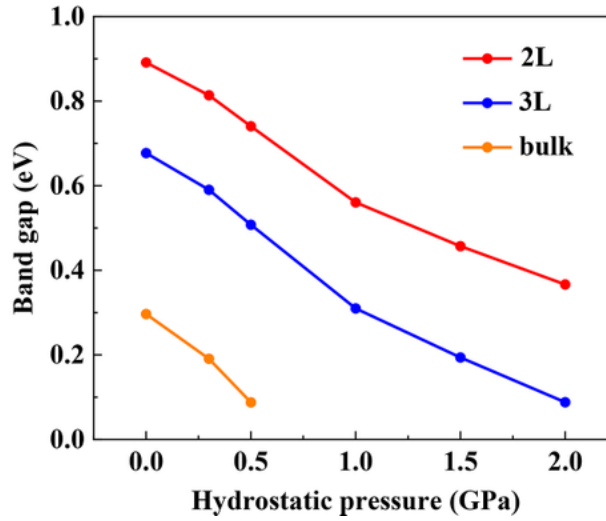
Figure I.5: Effect of hydrostatic pressure on the band gap of 2L, 3L, and bulk material [18].

- **2L** = Two layers of the material

- **3L** = Three layers of the material

- **Bulk** = The material in its three-dimensional (3D) bulk form

I.7.2 Empirical models for band gap variation [8, 10].

The pressure dependence of the band gap can be classified into two main models:

1. **Linear model:**

    When the quadratic coefficient (β) is negligible, the band gap follows a nearly linear relationship:

    $$E_g(\text{P}) \approx E_g(0) + \alpha \text{P} \tag{I.2}$$

    This model is often valid for low-pressure ranges where the band gap changes smoothly with compression.

2. **Nonlinear model**

At higher pressures, non-linear effects become more pronounced due to enhanced electronic interactions, requiring the inclusion of the βP^2 term. This modification more accurately captures the curvature of the band gap's evolution with pressure.

The values of α and β are determined through first-principles calculations or experimental measurements. The quadratic term βP^2 captures deviations from linear behaviour at higher pressures. Understanding these dependencies allows for the precise tuning of electronic properties, which is essential for optimising high-performance semiconductor devices and optoelectronic applications

I.8 Conclusion

This chapter provided a foundational overview of semiconductor materials, laying out their key types and physical characteristics. Both intrinsic and extrinsic semiconductors were examined, with a particular focus on compound materials especially the SiSn alloy, which stands out for its tunable properties and potential in advanced electronic applications.

In addition to the discussion on electronic band structures, the chapter highlighted the importance of direct and indirect band gaps in determining the optical and electronic performance of semiconductors. Several fundamental optical effects were also introduced, offering context for the use of these materials in devices like LEDs, solar cells, and sensors.

To conclude, we introduced first-principles methods such as Density Functional Theory (DFT), which are now essential tools in the study of material properties. The impact of external factors, particularly hydrostatic pressure, was briefly discussed establishing a foundation for the theoretical and computational approaches explored in the following chapter.

Chapter II:
Theoretical approaches using first-principles calculations

II.1 Introduction

The study of semiconducting materials has been significantly advanced by the development of computational methods grounded in quantum mechanics. First-principles calculations enable accurate predictions of structural, electronic, and optical properties without relying on empirical parameters. These techniques have become essential tools in materials science, offering detailed insights into material behaviour at the atomic scale [4, 19].

Among the most widely used computational frameworks is Density Functional Theory (DFT), which reformulates the complex many-body electron problem in terms of electron density rather than wave functions. This approach offers both practical and computationally efficient means of investigating the properties of complex materials, including semiconductor alloys [4, 17].

This chapter presents the theoretical methodologies applied in the study of materials, emphasising DFT and related computational techniques. The discussion includes the plane-wave pseudopotential method, theoretical modelling of the materials…etc

II.2 Schrödinger equation of a crystalline solid

Any crystalline solid can be considered as a single system composed of light particles (electrons) and heavy particles (nuclei). The stationary state of these particles is described by the Schrödinger equation [10]:

$$H\psi = E\psi \tag{II.1}$$

where H is the Hamiltonian of the crystal that contains all the energy terms (kinetic and potential energy), from both the nuclei and electrons. E is the total energy of the crystal, and ψ is the wave function of the system, which depends on the coordinates of the nuclei and electrons and contains all the information of the system [4, 10]:

$$\psi = (r_1, r_2, \ldots R_1, R_2, \ldots) \tag{II.2}$$

Here:

- r_i $(i = 1..N_e)$ are the coordinates of the electrons.

- N_e is the number of electrons.

- R_i $(i = 1....N_\alpha)$ are the coordinates of the nuclei.

- N_α is the number of atoms in the system.

The Hamiltonian operator includes all forms of energy, particularly:

1. The total kinetic energy of electrons [10]:

$$T_e = -\frac{\hbar}{2m_e}\sum_i \boldsymbol{\nabla}^2_{r,i} \tag{II.3}$$

2. The total kinetic energy of nuclei [4]:

$$T_n = -\frac{\hbar^2}{2M_i}\sum_i \boldsymbol{\nabla}^2_{R,i} \tag{II.4}$$

3. The interaction energy between electrons [4]:

$$V_e = \sum_{i<j}\frac{e^2}{|r_i-r_j|}v \tag{II.5}$$

4. The interaction energy between nuclei [4]:

$$V_n = -\sum_{\alpha<\beta}\frac{Z_\alpha Z_\beta e^2}{|\vec{R_\alpha}-\vec{R_\beta}|} \tag{II.6}$$

Where Z_α and Z_β are the charges of nuclei and , respectively.

5. The interaction energy between nuclei and electrons [4]:

$$V_{ne} = -\sum_{i,\alpha}\frac{Z_\alpha e^2}{|\vec{r_i}-\vec{R_\alpha}|} \tag{II.7}$$

The Schrödinger equation can thus be rewritten as:

$$(T_e + T_n + V_e + V_n + V_{ne})\psi(r_1, r_2, \ldots R_1 + R_2, \ldots) = E\psi(r_1, r_2, \ldots R_1 + R_2, \ldots) \quad (II.8)$$

This equation contains $3(Z+1)N_\alpha$ variables, and since there are about 10^{22} atoms in 1 cm³ of a crystalline solid, it is clear that obtaining an exact solution is impossible. It is a many-body problem that must be solved using a number of approximations. The first-order approximation is the Born-Oppenheimer or adiabatic approximation [1, 2].

II.3 Born-oppenheimer approximation

This approximation involves decoupling the motion of the nuclei from that of the electrons, which is justified by the fact that the mass of the nuclei is much greater than that of the electrons. Electrons are considered to be, at all times, in the ground state corresponding to the instantaneous positions of the nuclei. For particles as fast as electrons, the instantaneous positions of the nuclei are what matter. As for the nuclei, their motion is influenced only by the average behavior of all electrons, not by the instantaneous position of each one.

The roughest assumption is to consider the nuclei as immobile. This simplifies the Schrödinger equation by setting the kinetic energy of the nuclei to zero. The interaction energy between nuclei then becomes a constant, which can be set to zero by an appropriate choice of the origin. By considering $T_Z = 0$ and $U_Z = 0$, the electronic wavefunction ψ_e and a new Hamiltonian are defined as:

$$H = T_e + U_e + U_{ez} \tag{II.9}$$

The electronic Schrödinger equation becomes:

$$H_e \psi_e = E_e \psi_e \tag{II.10}$$

In this equation, as in the expression of ψ_e , R_α^0 appears as a parameter and not as a variable E_e .represents the energy of the electrons in the electric field of the fixed nuclei.

This approximation significantly reduces the number of variables required to describe the function . All terms in the Hamiltonian involving nuclei are eliminated. However, it is still insufficient to solve the Schrödinger equation due to the complexity of electron-electron interactions.

Therefore, it is often combined with the Hartree approximation. The Hartree-Fock approximation [13] assumes that each electron moves independently in an average field created by other electrons and nuclei. This reduces the N-electron problem to a set of   single-electron equations, replacing thetwo-particle potential$^1/r_{ij}$with a single-electron-dependent interaction:

$$V_i(r) = \sum_k \frac{-Ze^2}{|\vec{r_i} - \vec{R_k}|} \tag{II.11}$$

is the potential energy of electron in the field of nuclei k . $R_k$is the fixed position of nucleus$k$.

The Hartree effective field is:

$$V_H(r) = \frac{e^2}{4\pi\varepsilon_0}\sum_J \frac{1}{|\vec{r_i}-\vec{R_J}|} \tag{II.12}$$

This average crystal potential, V_{eff} includes the periodic contributions of the ions and electron interaction effects:

$$V_{eff}(r)=V_i(r)+V_H(r)+V_{xc}(r) \tag{II.13}$$

The energy of the electronic system is the sum of the individual energies:

$$\phi_e(r_1,r_2,\dots r_n) = \phi_e(r_1)\phi_2(r_2)\dots\phi_n(r_n) \tag{II.14}$$

with:

$$H_e\phi = E_e\phi \tag{II.15}$$

This transforms the multi-electron equation into a system of one-electron equations in the Hartree field:

$$\left[-\frac{\hbar}{2m}\nabla^2 + V_{eff}(r)\right]\phi_i(r) = \varepsilon_i\phi_i(r) \tag{II.16}$$

Since the electron is a fermion, the total wave-function must be antisymmetric under the exchange of two particles, which Hartree neglects. To correct this, Fock introduced the Pauli exclusion principle, and the electronic wave-function is expressed as a Slater determinant [7]:

$$\varphi(r_1\sigma_1, r_2\sigma_2,\dots\dots, r_{N_e}\sigma_{N_e}) = \frac{1}{\sqrt{N_e!}}\begin{vmatrix} \varphi_1(r_1\sigma_1) & \varphi_2(r_1\sigma_1) & \dots & \varphi_{N_e}(r_1\sigma_1) \\ \varphi_1(r_2\sigma_2) & \varphi_2(r_2\sigma_2) & \dots & \varphi_{N_e}(r_2\sigma_2) \\ \vdots & \vdots & \ddots & \vdots \\ \varphi_1(r_{N_e}\sigma_{N_e}) & \varphi_1(r_{N_e}\sigma_{N_e}) & \dots & \varphi_{N_e}(r_{N_e}\sigma_{N_e}) \end{vmatrix} \tag{II.17}$$

where $\frac{1}{\sqrt{N_e!}}$ is the normalization constant.

II.4 Density functional theory (DFT)

Density Functional Theory (DFT) is currently one of the most widely used methods for calculating the physical properties of materials. The main goal of DFT is to replace the many-electron wave function with the electron density as the fundamental quantity in calculations.

The principle of DFT lies in reformulating the N-body quantum problem into a single-body problem. The central idea is that the ground-state electron density of a system completely determines the expectation values of observables, such as the total energy [7].

II.4.1 Hohenberg-kohn theorems

The foundational formalism of DFT is based on the Hohenberg-Kohn theorems (1964) [7], which consist of two key theorems:

a. First theorem

The electron density $\rho(r)$ uniquely determines the external potential $V_{ext}(r)$ and consequently, all properties of the system. This implies that there is a one-to-one correspondence between the ground-state density $\rho_0(r)$ and the ground-state wave function φ_0. The total energy can be expressed as:

$$E = E_0[\rho_0] = F_{HK}[\rho_0] + \int V_{ext}(r)\,\rho(r)dr \qquad (II.18)$$

Where:

$$F_{HK}[\rho]=T[\rho]+V_{ee}[\rho] \qquad (II.19)$$

- $F_{HK}[\rho]$: The Hohenberg-Kohn functional.
- $T[\rho]$: Kinetic energy functional.
- $V_{ee}[\rho]$: Electron-electron interaction energy.

However, this theorem does not provide a practical method for determining whether a trial density corresponds to a ground state. This leads to the second theorem.

b. Second theorem

The energy functional $E[\rho]$ achieves its minimum for the true ground-state density $\rho_0(r)$. That is:

$$E_0[\rho_0]=min\,E[\rho] \qquad (II.20)$$

This implies that any trial density that is not the ground-state density will yield a higher energy:

$$\varphi_{test}|H|\varphi_{test}=E[\rho] \geq E_0=(\varphi_0|H|\varphi_0) \qquad (II.21)$$

Thus, all properties of a system defined by an external potential V_{ext} can be determined from the ground-state electron density. The energy E_ρ is minimized if and only if corresponds to the ground state.

A major challenge remains: how to express the Hohenberg-Kohn functional $F_{HK}[\rho]$ analytically for an interacting N-electron system.

The Hartree potential is given by:

$$V_H(r) = \frac{e^2}{2} \int \frac{\rho(r)\rho(r')}{|r-r'|} d^3r d^3r' \qquad (II.22)$$

The exchange-correlation potential is obtained as the functional derivative:

$$V_{xc}[\rho(r)] = \frac{\delta E_{xc}[\rho(r)]}{\delta\rho(r)} \qquad (II.23)$$

Under the influence of the effective potential, the Kohn-Sham equations are written as:

$$\widehat{H}\psi = \left[-\frac{\hbar}{2m}\nabla^2 + V_{eff}(r)\right]\psi_i(r) = E_i\psi(r) \qquad (II.24)$$

II.4.2 Kohn-sham equations

In the Kohn-Sham approximation of Density Functional Theory (DFT), the many-electron problem is reduced to a set of equations for non-interacting particles that reproduce the same electron density as the true system. The electron density is given by:

$$\rho(r) = \sum_i^{occ}|\phi_i(r)|^2 \qquad (II.25)$$

Each orbital $\psi_i(r)$ satisfies the Kohn-Sham equation:

$$\left[-\nabla^2 + V_{eff}(r)\right]\phi_i(r) = \varepsilon_i\phi_i(r) \qquad (II.26)$$

The effective potential $V_{eff}(r)$ consists of three terms:

$$V_{eff}(r) = e^2 \int \frac{\rho(r')}{|r-r'|} - \sum_i \frac{Ze^2}{|r-R_i|} + \frac{\delta E_{xc}[\rho(r)]}{\delta\rho(r)} \qquad (II.27)$$

The first term is the Hartree potential, the second term accounts for the nuclear attraction, and the last term is the exchange-correlation potential. These equations are solved self-consistently:

starting from a trial density, a new effective potential is computed, which yields new orbitals and hence a new density, and the process is repeated until convergence is achieved [19].

To ensure the Pauli exclusion principle is respected, the total wave function of the system is written as a Slater determinant of the single-particle orbitals ψi This construction guarantees antisymmetry under the exchange of two electrons, thus preventing any two electrons with the same spin from occupying the same quantum state.

II.5 The Exchange-correlation functional

In Density Functional Theory (DFT), the electron-electron interaction is accounted for using the exchange-correlation functional, which consists of two essential contributions:

- Exchange energy, which arises from the Pauli principle and describes the interaction between electrons of the same spin.

- Correlation energy, which represents the dynamic interactions between electrons due to Coulomb repulsion.

These interactions are complex and cannot be solved analytically. Therefore, several approximations of the exchange-correlation functional have been developed, including the Local Density Approximation (LDA) and the Generalized Gradient Approximation (GGA).

II.5.1 Local density approximation (LDA)

The Local Density Approximation (LDA) is one of the earliest and most commonly used approximations in DFT. It assumes that the exchange-correlation energy of an inhomogeneous system can be approximated by that of a homogeneous electron gas with the same local density. Mathematically, this approximation is given by:

$$E_{xc}^{LDA} = \int n(r)\varepsilon_{xc}\big(n(r)\big)dr \qquad (II.28)$$

where is the exchange-correlation energy per electron in a homogeneous electron gas of density. A more detailed formulation of the exchange energy in LDA is given by Dirac's approximation:

$$E_x^{LDA} = -C_x \int n(r)^{\frac{3}{4}} dr \qquad (II.29)$$

where is a spin-dependent constant. The correlation energy is often obtained using the Perdew-Zunger parameterization, based on Monte Carlo results from Ceperley and Alder:

$$E_c^{LDA} = \int n(r).\varepsilon_c(n(r))dr \tag{II.30}$$

This approximation is particularly effective for systems where the electronic density varies slowly in space. However, LDA has certain limitations: it tends to underestimate the band gaps of semiconductors and insulators and may overestimate cohesion in some materials. Despite these drawbacks, it remains widely used due to its low computational cost and reliable results for specific classes of materials.

II.5.2 Generalized gradient approximation (GGA)

The Generalized Gradient Approximation (GGA) improves upon LDA by incorporating not only the local electronic density but also its spatial gradient. It is defined by the expression:

$$E_{xc}^{GGA} = \int n(r).\varepsilon_{xc}(n.\nabla n)dr \tag{II.31}$$

where is a function explicitly dependent on the electronic density and its spatial variation. By considering local density fluctuations, GGA enhances the description of interatomic forces and partially corrects the underestimations of band gaps observed with LDA.

A commonly used GGA functional is Perdew, Burke, and Ernzerhof (PBE) [17], which offers a good balance between accuracy and computational cost. However, although it provides better descriptions of electronic structures and energetic properties, it still slightly underestimates band gaps compared to experimental values.

II.6 Numerical resolution of the kohn-sham equations

The Kohn-Sham equations are a set of single-electron Schrödinger-like equations that can be solved numerically using an iterative self-consistent procedure. The process begins with an initial guess for the electron density, which is used to evaluate the various density functionals and determine the effective potential using the equation:

$$v_{eff}(r) = v_{ext}(r) + v_{Hartree}(r) + v_{xc}(r) \tag{II.32}$$

where:

- $v_{ext}(r)$ is the external potential due to the nuclei,
- $v_{Hartree}(r)$ is the Hartree potential accounting for electron-electron Coulomb interactions,
- $v_{xc}(r)$ is the exchange-correlation potential.

25

Once is determined, the system of single-electron Kohn-Sham equations is solved to obtain new wave-functions, which in turn provide an updated electron density. This process is repeated iteratively until self-consistency is achieved, meaning that the difference between successive iterations is below a predefined convergence threshold [13, 15].

The iterative procedure is illustrated in **Figure II.1**, which describes the Self-Consistent Field (SCF) cycle used to solve the Kohn-Sham equations numerically [20].
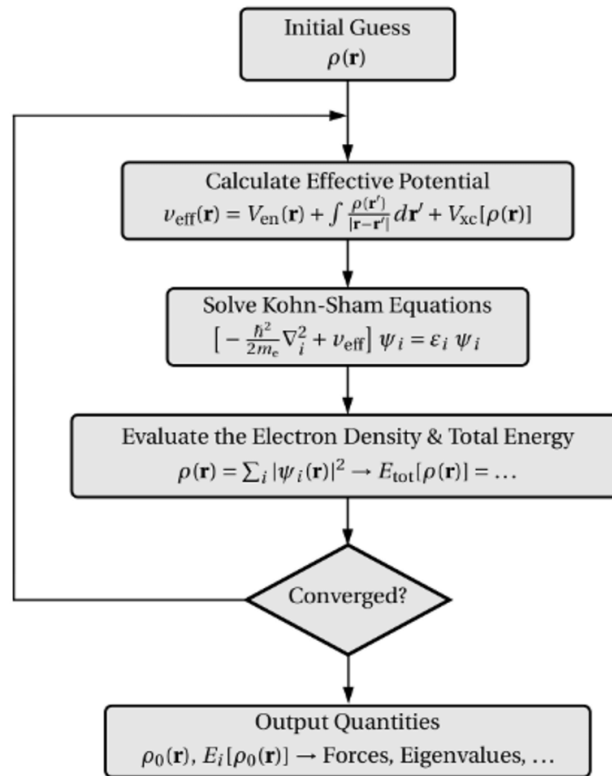
Figure II.1 Self-Consistent Field (SCF) cycle used to solve the Kohn-Sham equations numerically [20].

II.7 Pseudopotential and plane-wave methods

In the DFT formalism, certain many-body observables can be represented by single-particle observables. However, a significant challenge remains in handling an infinite number of non-interacting electrons moving within the static potential of an infinite number of nuclei or ions. At this stage, a wave-function must be computed for each electron among an infinite number within the system.

This problem can be addressed by applying Bloch's theorem to the electronic wave-function, which naturally leads to the use of a plane-wave basis and the special k-point sampling technique in reciprocal space [13]. The plane-wave basis provides a convenient mathematical

framework, ensuring accurate and efficient computations while maintaining the translational symmetry of the crystal.

By using pseudopotentials, the complexity of dealing with core electrons is reduced, allowing only valence electrons to be explicitly considered in calculations. This significantly improves computational efficiency and accuracy in determining the electronic structure of semiconducting materials [10]

II.8 Bloch's theorem

The symmetry properties of crystals, particularly translational invariance in the direct lattice, imply that the Hamiltonian in the Kohn-Sham formalism commutes with the translation operator. This leads to the well-known Bloch theorem, which states that the wave-function of an electron in a periodic potential can be written as a product of a plane wave and a function that has the periodicity of the crystal lattice [4, 10]:

$$\psi_{nk}(\text{r}) = e^{i\,k.r}u_{nk}(\text{r}) \tag{II.33}$$

where:

- $u_{nk}(\text{r})$ is a periodic function satisfying $u_{nk}(r+R) = u_{nk}(r)$ for any lattice translation vector,

- k is the wave vector in the first Brillouin zone of the reciprocal lattice.

The periodic function $u_{nk}(\text{r})$ can be expanded as a sum of reciprocal lattice vectors:

$$u_{nk}(\text{r}) = \sum_G C_{nk}(G)e^{i(G)r} \tag{II.34}$$

Where G is a reciprocal lattice vector defined by the condition $G * R = 2\pi m$ with m being an integer [10, 17].

Thus, the total wave-function can be expressed as a sum of plane waves:

$$\psi_{nk}(\text{r}) = \sum_G C_{nk}(G)e^{i(k+G)r} \tag{II.35}$$

Bloch functions describe electron wave-functions in a periodic potential, where the plane wave term represents a free-electron-like behaviour, and modulates this wave according to the periodicity of the lattice potential. In band structure calculations, each -point in the Brillouin

zone corresponds to multiple solutions of the Schrödinger equation, forming distinct energy bands [10, 13].

II.9 Plane-wave basis expansion

The most natural way to represent wave-functions in DFT calculations is through a plane-wave expansion. Plane waves offer several advantages, including a simple mathematical formalism and the ability to form a complete basis set [10].

By using such a decomposition, the Kohn-Sham equations can theoretically be solved efficiently. However, two main challenges arise when using plane waves in practice:

1. There is an infinite number of reciprocal lattice vectors G that contribute to the expansion.

2. The number of k-points in the first Brillouin zone is also infinite [10].

To address the first problem, a cutoff energy is introduced, beyond which plane waves are not included in the calculation. This restriction helps limit the number of plane waves needed while maintaining accuracy. The condition for selecting the plane waves is defined by the following equation [10]:

$$\frac{\hbar^2}{2m}|k + G| \leq E_{Cut} \tag{II.36}$$

where:

- k is the wave vector,
- G is a reciprocal lattice vector.
- m is the electron mass.
- $\hbar$ is Planck's constant.
- E_{cut} is the cut-off energy.

The E_{cut} choice of depends on the system under study and, in particular, on the pseudopotential used to describe the core-valence interaction. If E_{cut} is too low, the number of plane waves in the calculation will be insufficient to accurately describe the wave-functions and charge density. However, increasing significantly raises computational costs. Therefore, it is necessary to find an optimal balance where the total energy of the system converges within the required precision limits [10].

Using a plane-wave basis provides several key advantages [10]:

- Controlled Convergence: The accuracy of physical properties can be systematically improved by increasing the number of plane waves.

- Simplified Force Calculations: Forces acting on atoms can be easily derived from the wave-functions.

- Uniform Spatial Representation: Since plane waves uniformly describe space, they eliminate issues related to basis set superposition errors.

- Efficient fourier transform usage: Plane-wave methods leverage Fast Fourier Transforms (FFT) to transition between real and reciprocal space, making computations highly efficient. FFT operations are optimized on most modern computing architectures, further reducing computational costs.

The second challenge-handling an infinite number of k-points in the Brillouin zoneis addressed by employing an appropriate Brillouin zone sampling scheme, such as the Monkhorst-Pack method [11].

II.10 Pseudopotentials

The use of pseudopotentials within the DFT formalism has demonstrated considerable success in recent years for calculating and predicting the ground-state properties of solids.

The fundamental idea behind the pseudopotential method is to describe only the valence states of a system (atoms, molecules, or crystals) without explicitly considering the core states, which are not essential for determining most physical properties. This is known as the frozen-core approximation, which assumes that core electron states remain unchanged by variations in the surrounding electronic configuration [10].

In practice, the wave-functions of valence electrons are replaced by smoother pseudo wave-functions, which eliminate the need to account for core electron oscillations due to orthogonality constraints. This substitution is imposed outside a critical radius around the nucleus, ensuring that beyond this radius. Within this region, the pseudo wave-functions are designed to remove rapid oscillations and simplify numerical computations [10].

These pseudowave-functions have the advantage of being represented in Fourier space with a significantly reduced number of plane waves, which leads to substantial computational savings.
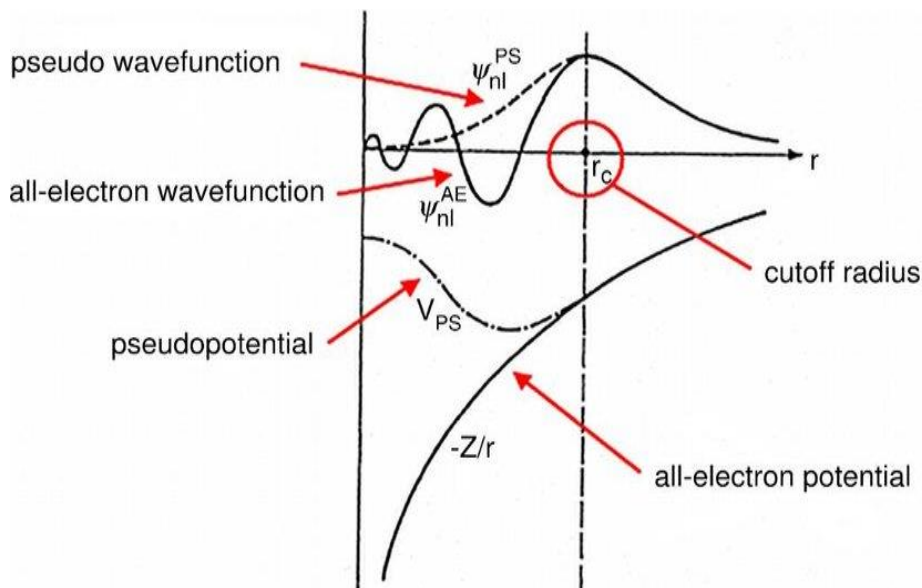
Figure II.2. Illustrates the comparison between an all-electron potential and its corresponding pseudopotential, as well as the difference between exact and pseudo wave-functions [21].

The pseudopotential is constructed so that the pseudo wave-functions and the original valence wave-functions maintain the same eigenvalues.

The interaction between valence electrons and the ionic core includes:

- The Coulomb interaction between valence electrons and nuclei, screened by core electrons,

- Valence-core repulsion, dictated by the Pauli exclusion principle,

- Exchange-correlation effects, which influence the electronic structure of the material [10].

II.11 Brillouin zone sampling

Sampling the first Brillouin zone is a critical step in Density Functional Theory (DFT) calculations, as it directly affects the accuracy of integrals performed over reciprocal space. This is particularly important when evaluating electronic properties such as the density of states (DOS) and total energy, which require summation over discrete k-points within the Brillouin zone.

While increasing the number of k-points enhances the precision of these calculations, it also raises computational cost and memory demands. Therefore, achieving an optimal balance between accuracy and efficiency is essential [10]. In this study, the Monkhorst–Pack scheme is

employed to systematically generate a grid of k-points, allowing for accurate numerical integration while maintaining computational feasibility.

II.12 Cutoff energy

The cutoff energy E_{cut} is a critical parameter in plane-wave-based DFT calculations. It represents a convergence criterion used to minimize errors in the approximation of the kinetic energy of electrons. In the plane-wave expansion method, the basis set is truncated by limiting the reciprocal space representation to a sphere of radius $|k + G|$ ensuring computational efficiency while maintaining accuracy.

The kinetic energy of a plane wave is defined as:

$$E_{cut} = \frac{\hbar^2}{2m}|k + G|^2 \tag{II.37}$$

Where:

- k is the wave vector,
- G is a reciprocal lattice vector,
- $\hbar$ is the reduced Planck's constant,
- m is the electron mass.

The total number of plane waves included in the basis set increases with E_{cut} and is approximately determined by:

$$N_{PW} \propto N_k \cdot \frac{V}{(2\pi)^3} \tag{II.38}$$

- N_k is the number of k-points in the Brillouin zone sampling
- V is the volume of the unit cell.

The figure II.3 shows how the total energy stabilizes as the cutoff increases, helping determine the optimal balance between accuracy and computational cost.
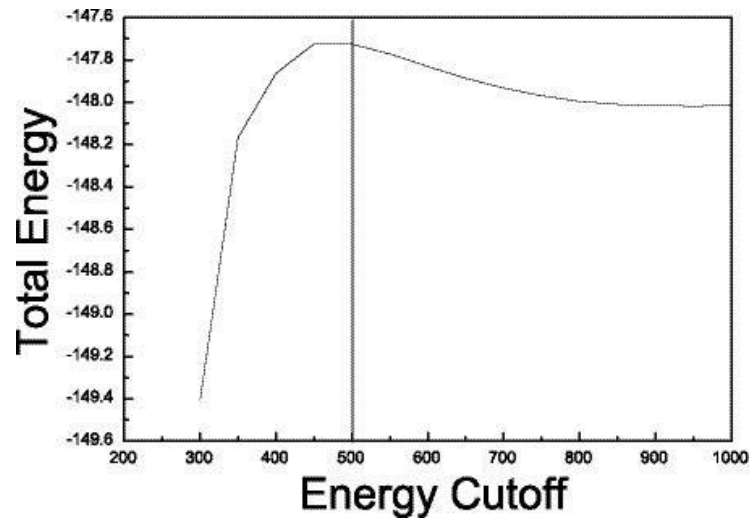
Figure II.3. Convergence of the total energy with respect to the plane-wave cut-off energy [22].

This figure illustrates the dependence of the total energy of the SiSn alloy on the plane-wave cut-off energy, with both quantities expressed in electronvolts (eV). As the cut-off energy increases, the total energy progressively approaches a constant value, indicating that convergence has been achieved. This confirms the suitability of the chosen cut-off for accurate and efficient simulations.

II.13 Conclusion

This chapter has outlined the theoretical methods used in predicting material properties, highlighting the application of density functional theory (DFT) and its associated computational techniques. The use of pseudopotential methods and plane-wave expansions enhances computational efficiency while maintaining high accuracy in predicting material properties such as structural optimisation, equilibrium lattice parameter, band structure…. etc.

Chapter III:

Calculation method, results presentation and their discussion

III.1 Introduction

The SiSn alloy, with its cubic zinc-blende structure, is a promising material for optoelectronic applications. A comprehensive understanding of its structural, electronic and optical properties is crucial for potential technological advancements. This chapter presents the theoretical methodologies applied in the study of SiSn, the impact of hydrostatic pressure, and the use of the CASTEP simulation package [23]. The insights derived from these methods form the foundation for analyzing the behavior of SiSn under different conditions [7, 14].

The present study investigates the electronic properties of the SiSn alloy in the cubic zinc-blende (F$\overline{4}$3m) phase, using Density Functional Theory (DFT) with the norm-conserving pseudopotential method as implemented in the CASTEP software [23]. The Local Density Approximation (LDA) was employed for exchange-correlation interactions, which, despite its tendency to underestimate band gaps, provides reliable predictions for structural and electronic properties [17].

To analyse the impact of external pressure, calculations were performed at P = 0 GPa and P = 8 GPa. Previous studies show that pressure can modify the band structure, density of states (DOS), and carrier mobility [24], making SiSn a promising candidate for strain-engineered semiconductor devices [17]. The choice of LDA ensures an optimal balance between accuracy and computational efficiency, particularly for IV-IV semiconductor alloys [5].

These findings contribute to the understanding of SiSn's pressure-dependent electronic behaviour, which is crucial for its potential applications in optoelectronics and high-performance semiconductors [5, 24].

III.2 CASTEP code

CASTEP (Cambridge Serial Total Energy Package) is a first-principles simulation software based on Density Functional Theory (DFT). It enables the calculation of total energies, atomic forces, stress tensors, optimized geometries, band structures, optical spectra, and elastic constants of semiconducting materials [19]. CASTEP was developed by Professor K. C. Payne and is commercially distributed by Accelrys.

CASTEP employs the pseudopotential and plane-wave (PP-PW) method to solve the Kohn-Sham equations in the DFT framework. This approach allows accurate modeling of semiconducting materials by incorporating the influence of exchange-correlation interactions through the Local Density Approximation (LDA) [25,26]. The software uses a special k-point

integration method in the first Brillouin zone to compute electronic properties efficiently. The Monkhorst-Pack grid is used to optimize the k-point sampling, ensuring precision in band structure calculations [24].

Additionally, CASTEP employs a density-mixing algorithm to iteratively solve the Kohn-Sham equations, minimizing the total energy and allowing ionic relaxation under the influence of interatomic forces. The Fast Fourier Transform (FFT) technique is utilized to efficiently transform wave-functions and potentials between real and reciprocal space, significantly reducing computational costs and optimizing resource usage [19].

For the semiconducting materials alloy, CASTEP has been employed to calculate:

- Lattice parameters to determine structural stability.

- Electronic band structures and density of states (DOS) to analyze semiconductor properties.

- Optical properties such as absorption and dielectric function to assess potential applications in optoelectronics [24].

These simulations provide valuable insights into the electronic and optical behavior of semiconducting materials, contributing to its potential use in semiconductor and high-performance electronic applications [4,10,14].

III.3 Structural properties

III.3.1. Input parameters

The accuracy of CASTEP simulations depends on a set of fundamental input parameters that define the material's atomic structure and computational settings. These include:

1. The chemical composition of the system;

2. The crystallographic space group and lattice parameters;

3. The plane-wave energy cutoff (Ecut) and Brillouin zone sampling (nkpt), which ensure numerical accuracy.

For the SiSn alloy, these parameters are summarized in **Table III.1**.

<div align="center">**Table III.1. Input parameters of the studied SiSn alloy**</div>

Material	Lattice Constant (Å)	Angles (°)	Space Group	Atomic Number
SiSn	a = **5.90**	$\alpha = \beta = \gamma = 90°$	216 (F$\overline{4}$3m)	Si: 14, Sn: 50

The atomic arrangement of the SiSn alloy in the zinc-blende (F$\overline{4}$3m) phase is illustrated in **Figure III.1.** This structure consists of two interpenetrating face-cantered cubic (FCC) sub lattices, where Si and Sn atoms alternate, forming a tetrahedral coordination. The red and green spheres represent Si and Sn atoms, respectively.
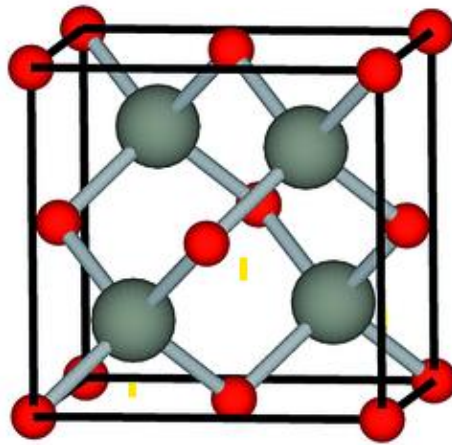
<div align="center">**Figure III.1.** Conventional unit cell of the SiSn alloy in the zinc-blende phase [27].</div>

To accurately describe exchange-correlation interactions, the Local Density Approximation (LDA) within DFT is employed. Although LDA tends to underestimate band gaps, it provides reliable structural properties, making it suitable for this study.

III.3.2. Convergence tests

Before analysing the physical properties of the SiSn alloy, convergence tests were conducted to determine the optimal computational parameters. We tested the convergence of the results with respect to the cutoff energy E_{cut} and the Brillouin zone sampling (the number of k-points). To determine reliable values of E_{cut} and k-points that ensure the convergence of the system's total energy, we varied E_{cut} from 200 to 900 eV. After each test, the total energy was recorded, and the variation of the total energy as a function of E_{cut} is plotted in Figure **III.2 (a)**.

Once the optimal E_{cut} value was determined, we proceeded with the sampling of the Brillouin

zone by varying the number of k-points. The variation of the total energy as a function of the number of k-points is shown in Figure **III.2 (b)**. From these plots, we observe that a cutoff energy of $E_{cut} = 400$ eV and a k-point grid of $8 \times 8 \times 8$ sufficiently ensure good convergence of the total energy.

These optimizations ensure a balance between accuracy and computational efficiency, providing a reliable foundation for further analysis of the structural, electronic, and optical properties of the SiSn alloy.
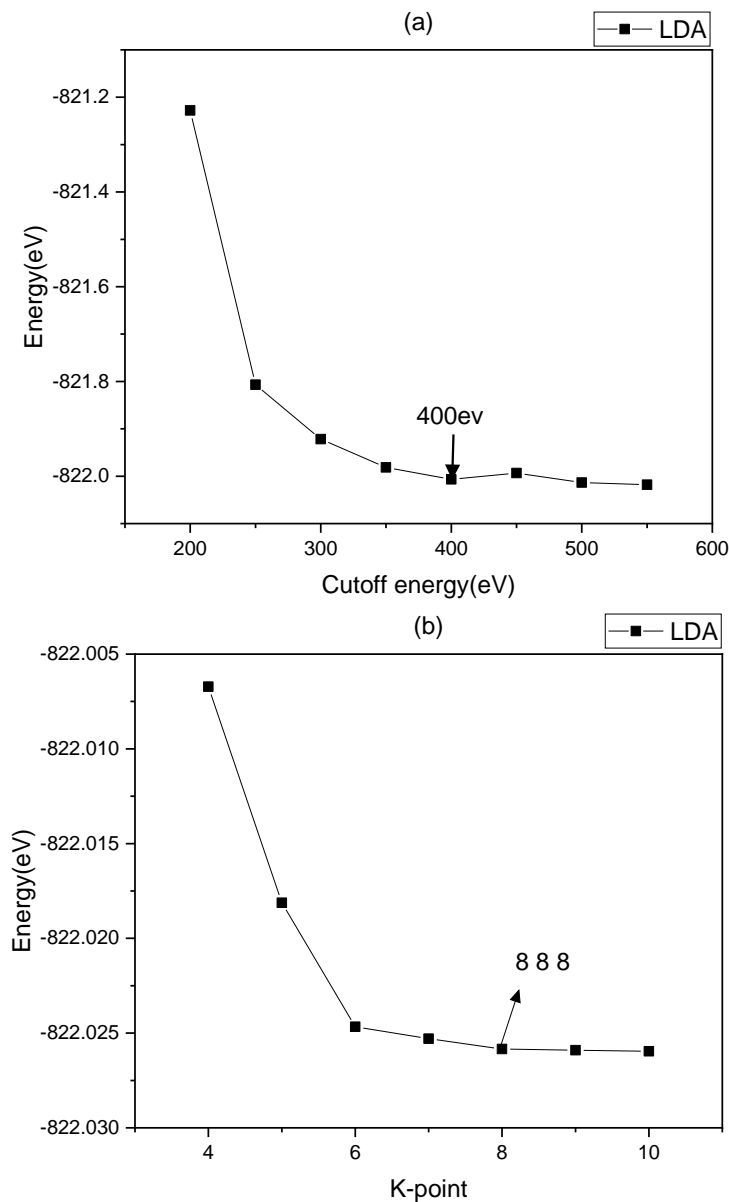
Figure III.2. Variation of the total energy of the SiSn alloy as a function of (a) the cutoff energy E_{cut} and (b) the number of k-points.

III.3.3. Equation of state parameters

The study of structural properties is fundamental in first-principles calculations, as all other quantities, such as mechanical, electronic, and optical properties, are directly related to them. To achieve this, we first determined the structural properties at equilibrium (P = 0 GPa and T = 0 K) of the SiSn alloy in its cubic zinc-blende phase.

To obtain key material parameters, such as the equilibrium unit cell volume (V_0), the bulk modulus (B_0), and its pressure derivative (B_0'), a geometric optimization was performed at different pressures. At each step, the **t**otal energy and the corresponding volume were recorded. The values of V_0, B_0 and B_0' were then obtained by fitting the energy-volume (E-V) data using Murnaghan's equation of state [28]:

$$E(V) - E(V_0) = \frac{B_0 V}{B'_0} \left[\frac{\left(\frac{V_0}{V} \right)^{B'_0}}{B'_0 - 1} + 1 \right] - \frac{B_0 V}{B'_0 - 1} \tag{III.1}$$

where $E(V_0)$ is the energy corresponding to the equilibrium volume V_0.
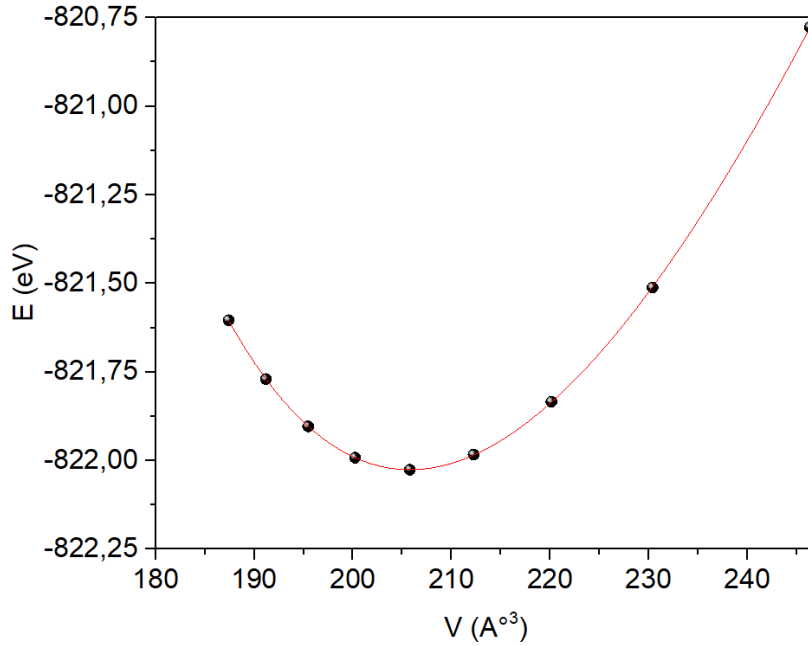

Figure III.3. Variation of the total energy of the SiSn alloy as a function of unit cell volume.

The obtained values for the lattice constant a_0, the bulk modulus B_0, and its pressure derivative B_0' are summarized in **Table III.2**.

Additionally, these parameters can also be determined by fitting the pressure-volume (P-V) data using Birch-Murnaghan's equation of state [29]:

$$.P(V) = \frac{3}{2}B_0 \left[\left(\left(\frac{V_0}{V} \right)^{\frac{7}{3}} - \left(\frac{V_0}{V} \right)^{\frac{5}{3}} \right) \right] \left[1 + \frac{3}{4}(B'_0 - 4) \left(\left(\frac{V_0}{V} \right)^{\frac{2}{3}} - 1 \right) \right]$$

(III.2)

The response of the binary SiSn alloy to external pressure has been analysed by investigating the dependence of the unit cell volume under applied hydrostatic pressure. Our results are presented in **Figure III.4**. It is observed that the unit cell volume decreases monotonically with increasing pressure
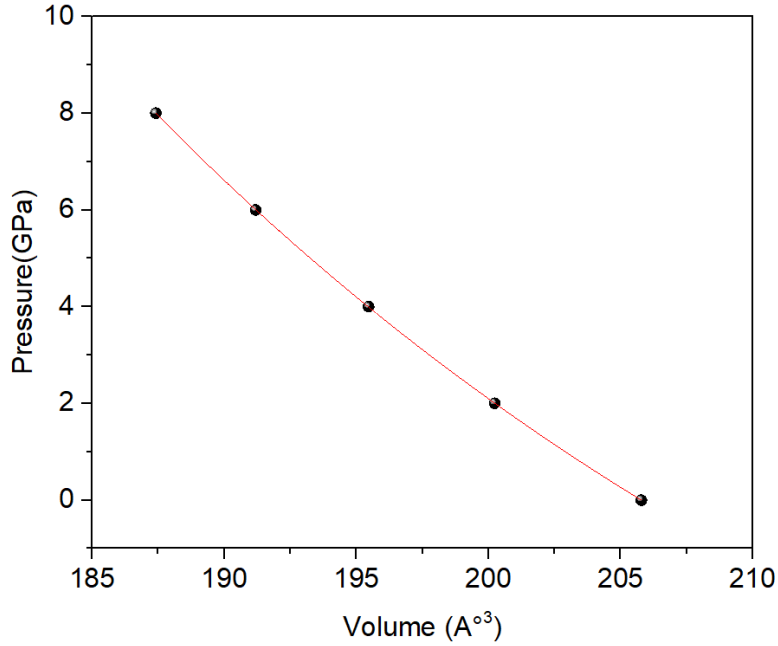
Figure III.4. Pressure-volume dependence of the SiSn alloy using the LDA approximation.

At zero pressure, the unit cell volume of SiSn is approximately 205 Å³**.** As pressure increases, the volume gradually decreases, reaching a value of 185 Å³ at 8 GPa**.** This behaviour aligns with the general trend observed in semiconductor alloys, where external pressure leads to a compression of the crystal lattice due to enhanced interatomic interactions [1, 2, 24].

Using the Birch-Murnaghan equation of state, the obtained values of a_0, B_0 and B_0' for the SiSn alloy are summarized also in **Table III.2**. Our findings are consistent with previous theoretical studies [5, 24].

Table III.2: Structural parameters of the SiSn alloy obtained using LDA.

Parameter	LDA (E-V Fit)	LDA (P-V Fit)	Ref. [5] LDA	Ref. [24] LDA
a_0 (Å)	5.90	5.90	5.904	5.81
B_0 (GPa)	69.78	68.93	68.554	72.47
B_0'	4.56	4.60	4.446	4.4

From these results, we observe that the lattice parameter a_0 obtained through equation of state fitting (E-V and P-V) are very close, confirming the reliability of our approach.

Furthermore, it is well known that the local density approximation (LDA) tends to underestimate the lattice parameter while overestimating the bulk modulus, which is consistent with our findings and previous studies on similar IV-IV semiconductor alloys [5, 24].

III.3.4. Theoretical mass density

One of the fundamental characteristics of crystals is their periodic arrangement of atoms or molecules [3]. This periodic structure defines and explains various physical properties of crystals, including their density. The crystal density (or theoretical density) g is given by the following relation [15]:

$$g = \frac{n \cdot M}{N_A \cdot V} \tag{III-3}$$

where:

- M is the molecular mass.
- N_A is Avogadro's number ($N_A = 6.022 \times 10^{23}$ mol^{-1}),
- n is the number of molecules per unit cell.
- V is the unit cell volume.

The theoretical density g of a solid corresponds to its average mass per unit volume. It is usually expressed in grams per cubic centimetre (g/cm³) or kilograms per cubic meter (1g/cm³=10 kg/m³).

For the SiSn alloy in the zinc-blende phase, the molar mass is given by:

$$M=4 \times M_{Si}+4 \times M_{Sn}=4 \times 28.085+4 \times 118.71$$

$$M=587.18 \text{ g/mol} \tag{III-4}$$

Thus, the theoretical density can be expressed as:

$$g(V)=\frac{587.18}{V}(\text{g/cm}^3) \tag{III-5}$$

The variation of the theoretical density g as a function of the unit cell volume V for the SiSn alloy is calculated using equation (III-5). **Figure III.5** illustrates the dependence of the theoretical density on pressure for this alloy. It can be observed that the theoretical density starts at approximately 4.7 g/cm³ at P = 0 GPa and increases with pressure, reaching around 5.2 g/cm³ at P = 8 GPa. This trend is consistent with previous studies on other semiconductors, which show an increase in density under compression due to reduced interatomic spacing [3,15].

Additionally, first-principles studies based on Density Functional Theory (DFT) have shown that changes in lattice constant under pressure significantly impact the structural and electronic properties of materials [4, 24]. These findings align with experimental results on density variations in related materials, such as SiGe and GeSn, where increasing pressure leads to higher densities due to structural compression [17].
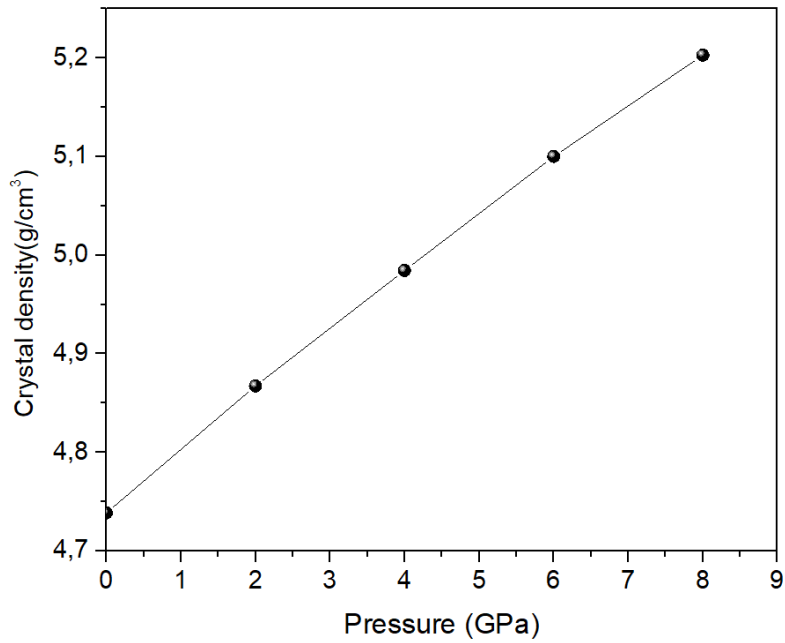
Figure III.5. Effect of pressure on the theoretical density g of the SiSn alloy.

The variation of the theoretical density as a function of pressure can be approximated using a quadratic function of the form [15]:

$$g(p) = g(0) + ap + bp^2 \qquad \text{(III-6)}$$

For the SiSn alloy, the interpolation of the theoretical density data gives the following equation:

$$g(p) = 4.74 + 0.066\,p - 9.63 \times 10^{-4}p^2$$

where g is expressed in g/cm³ and p in GPa.

Additionally, the theoretical density can also be expressed as a function of the relative lattice parameter (a/a_0) [15]. The obtained values of (a/a_0) and the corresponding theoretical density g of the SiSn alloy are summarized in **Table III.3**.

Table III.3. Theoretical density g as a function of the relative lattice parameter (a/a_0) for the SiSn alloy.

(a/a_0)	1.000	0.985	0.970	0.955	0.940	0.925	0.910	0.895	0.880
g (g/cm³)	4.74	4.82	4.90	4.98	5.05	5.11	5.17	5.22	5.27

Figure III.6 shows the dependence of the theoretical density g of the SiSn alloy on the relative lattice parameter (a/a_0) From this curve, we observe that the theoretical density decreases monotonically with increasing (a/a_0). This trend is directly correlated with pressure, as increasing pressure reduces the lattice parameter, leading to a decrease in (a/a_0) and an increase in density [15].
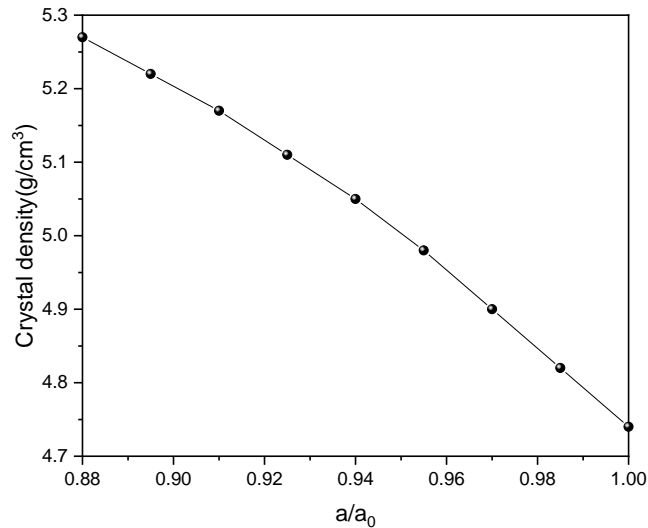

Figure III.6. Dependence of the theoretical density g of the SiSn alloy on the relative lattice parameter (a/a_0).

III.4. Electronic band structures

In a crystal, atoms arrange themselves in a regular pattern according to a triply periodic lattice, leading to a specific organization of electron energy levels. These electrons occupy well-defined states, forming allowed energy bands separated by forbidden bands where no electronic states exist. These band structures are represented in reciprocal space and are crucial for analysing the electronic properties of the studied material [1, 2].

The fundamental energy gap, or band gap, is defined as the difference between the maximum of the valence band (VBM) and the minimum of the conduction band (CBM). This property plays a key role in classifying materials as conductors, semiconductors, or insulators [7,14].

The electronic properties of the SiSn alloy in the zinc-blende structure were investigated using the pseudopotential plane-wave method within the Local Density Approximation (LDA). It is well known that LDA systematically underestimates the band gap [19, 21]. The electronic band structures were obtained by computing the Kohn-Sham orbitals along high-symmetry directions in the Brillouin zone. **Figure III.7** presents the band structures at 0 GPa and under an applied pressure of 8 GPa.
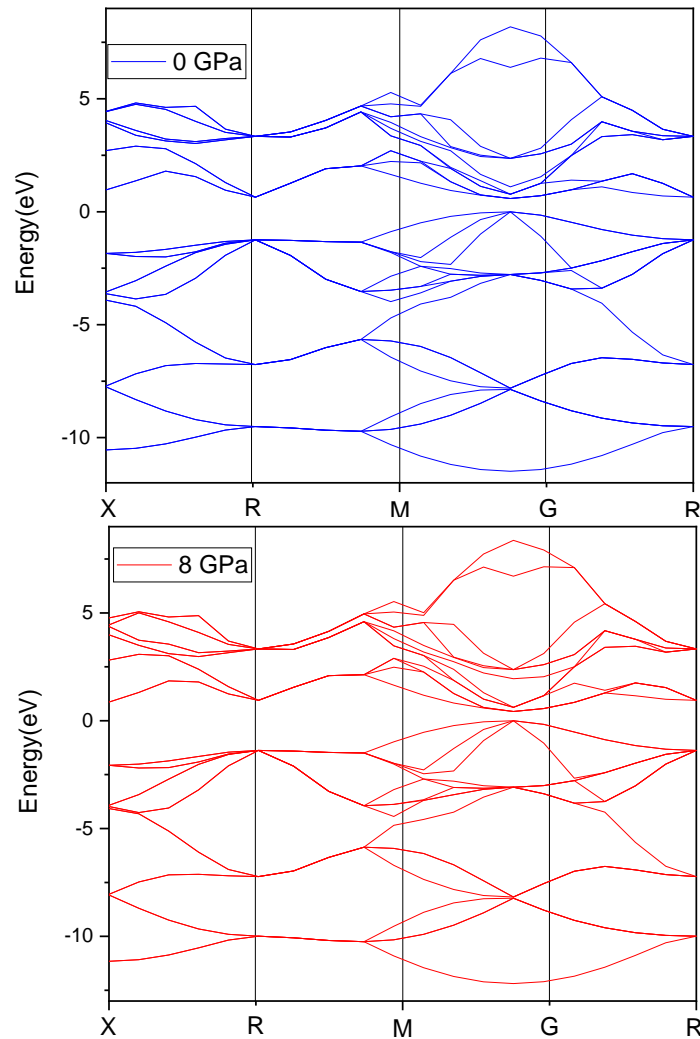
Figure III.7. Electronic band structures of the SiSn alloy at P = 0 GPa and P = 8 GPa.

Analysis of the results reveals that applying a pressure of 8 GPa significantly modifies the energy bands. In particular, a shift in conduction band levels and an alteration in band curvatures can be observed. However, the overall shape of the diagrams remains unchanged, indicating that pressure primarily affects interatomic distances and electronic coupling without inducing a radical electronic transition.

As expected, the LDA approximation underestimates the band gap, potentially leading to a semi-metallic behaviour instead of the expected semiconductor nature [19, 21]. From **Figure III.7**, the estimated band gap Eg of the SiSn alloy at P = 0 GPa is approximately 0.54 eV, which is consistent with the value 0.539 eV reported by Badal H. Elias [5]. This result is slightly lower than the values 0.91 eV and 0.9 eV reported by Zaoui *et al.* [4], Amrane *et al.* [17] Huang *et*

al. [30], respectively. The underestimation is expected due to the known limitations of the LDA method. This underestimation is well-documented and is attributed to the simplified treatment of electronic interactions in DFT-LDA [10, 19].

Applying external pressure reduces the band gap and modifies electron dispersion within the band structure. This phenomenon can impact optoelectronic and electronic transport applications, requiring adjustments for devices operating under pressure [15, 24].

III.5. Optical properties

In this study, we employ DFT within the LDA to investigate various optical properties as a function of photon energy. These properties include the refractive index, extinction and absorption coefficients, electron energy loss function, and optical conductivity, which is derived from the dielectric function

III.5.1. Dielectric function

The dielectric function ε(ω) is a complex function that characterizes the interaction between an electromagnetic wave and a material. It is expressed as:

$$\varepsilon(\omega) = \varepsilon_1(\omega) + i\varepsilon_2(\omega)$$ (III-7)

where:

- $\varepsilon_1(\omega)$ is the real part, which describes dispersion .

- $\varepsilon_2(\omega)$ is the imaginary part, which represents absorption.

Imaginary part of the dielectric function

The imaginary part $\varepsilon_2(\omega)$ is obtained from the electronic band structure using the expression [16]:

$$\varepsilon_2(\omega) = \frac{4\pi^2 e^2}{m^2\omega^2} \sum_{c.v} \int |M_{cv}(k)|^2 \, \delta(E_C(k) - E_v(k) - \hbar\omega) d^3k$$ (III-8)

where:

- e is the electron charge,

- m is the electron mass,

- ω is the photon frequency,

- $E_C(k)$ and $E_V(k)$ are the conduction and valence band energies, respectively,

- $|M_{cv}(k)|$ is the dipole matrix element **.**

- The integral runs over the Brillouin zone (BZ)**.**

Real part of the dielectric function

The real part $\varepsilon_1(\omega)$ is computed using the Kramers-Kronig relation:

$$\varepsilon_1(\omega) = 1 + \frac{2}{\pi} P \int_0^\infty \frac{\omega' \varepsilon_2(\omega')}{\omega'^2 - \omega^2} d\omega' \tag{III-9}$$

Where P represents the Cauchy principal value of the integral.

Figure III.8 shows the variations of the dielectric function $\varepsilon(\omega)$ of the SiSn alloy as a function of photon energy.

- At low photon energies, $\varepsilon_1(\omega)$ reaches its maximum near the absorption edge.

- The general shape of $\varepsilon_1(\omega)$ resembles a harmonic oscillator, with a resonance frequency near 6 eV.

- Applying P = 8 GPa shifts this resonance frequency to higher energy values, indicating pressure-induced modifications of the electronic band structure**.**

This behaviour is consistent with previous first-principles studies on semiconductor alloys [16, 19, 24], confirming the effect of pressure on optical transitions.
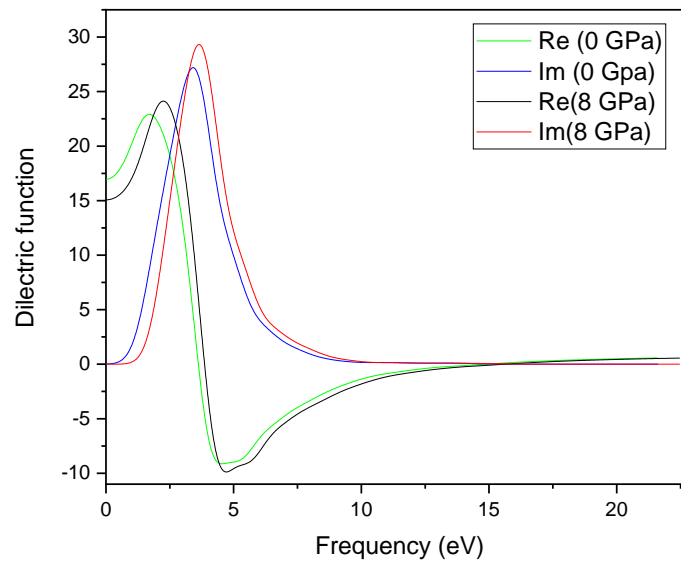
Figure III.8. Variations of the dielectric function $\varepsilon(\omega)$ of the SiSn alloy as a function of photon energy.
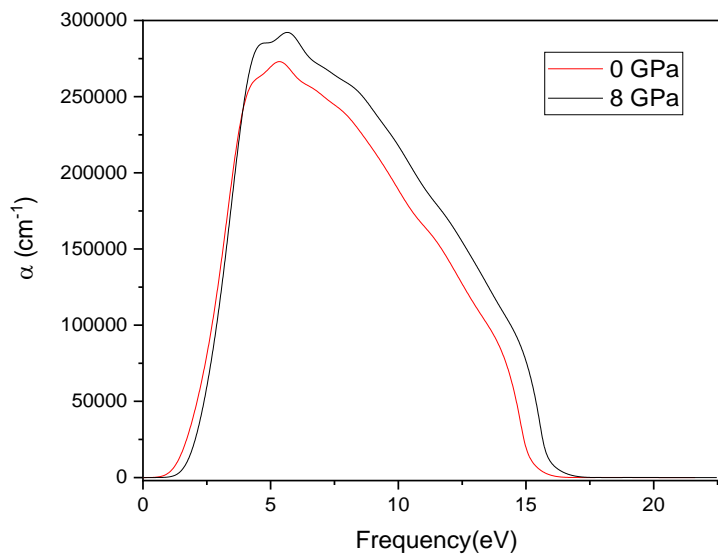
III.5.2. Optical absorption coefficient

The optical absorption coefficient α(ω) is a key parameter for understanding the penetration depth of light in a material and its interaction with electronic states. It is directly related to the material's band structure, indicating the onset of inter band transitions and the energy range where photon absorption occurs [16, 19].

In **Figure III.9**, we present the calculated absorption spectra for the SiSn alloy at P = 0 GPa and P = 8 GPa. The spectra show a broad absorption peak, highlighting two main regions of strong optical activity:

- At P = 0 GPa, the first peak appears at approximately 6 eV, corresponding to direct interband transitions.

- The absorption coefficient decreases after 15 eV, reaching near-zero values beyond this energy.

Upon applying P = 8 GPa, the absorption peak shifts to higher energies, indicating an increase in the bandgap due to pressure-induced modifications in the electronic band structure [19, 24]. Additionally, the peak intensity increases slightly, suggesting enhanced optical absorption in this energy range. Similar shifts under pressure have been observed in other group-IV semiconductors, including Si-Ge-Sn alloys [24].

These results confirm that external pressure can tune the optical absorption of the SiSn alloy, which is essential for applications in infrared detectors, photovoltaics, and optoelectronic devices [16, 19, 24].

Figure III.9. Optical absorption coefficient spectra α(ω) of the SiSn alloy at P = 0 GPa and P = 8 GPa as a function of photon energy.
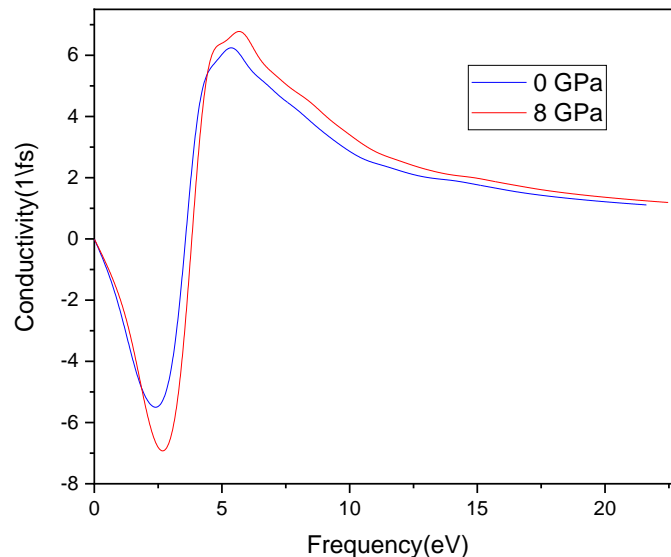
III.5.3. Optical conductivity

The optical conductivity$\sigma(\omega)$ is a fundamental parameter for characterizing the electronic response of a material to an external electromagnetic field. It provides insights into inter band transitions and the dynamical behaviour of charge carriers in semiconductors [16, 19].

In **Figure III.10**, we present the calculated optical conductivity $\sigma(\omega)$ of the SiSn alloy at P = 0 GPa and P = 8 GPa as a function of photon energy. The spectra exhibit two distinct peaks, indicating the presence of strong electronic transitions:

- The first peak appears at approximately 6 eV, corresponding to the fundamental inter band transitions.

- The second peak, located at higher photon energies, is associated with additional electronic excitations and the influence of conduction band states.

Under applied pressure (P = 8 GPa)**,** the first peak shifts slightly toward higher energies, suggesting an increase in the electronic bandgap and changes in electron mobility [19, 24]. Additionally, the second peak exhibits a reduction in intensity, which may indicate a decrease in optical absorption at higher photon energies. Similar behaviour has been observed in II-VI semiconductors and strained Si-based alloys [16, 19, 24].

These results demonstrate that external pressure modifies the optical response of the SiSn alloy, making it a promising material for pressure-tenable optoelectronic applications [19].
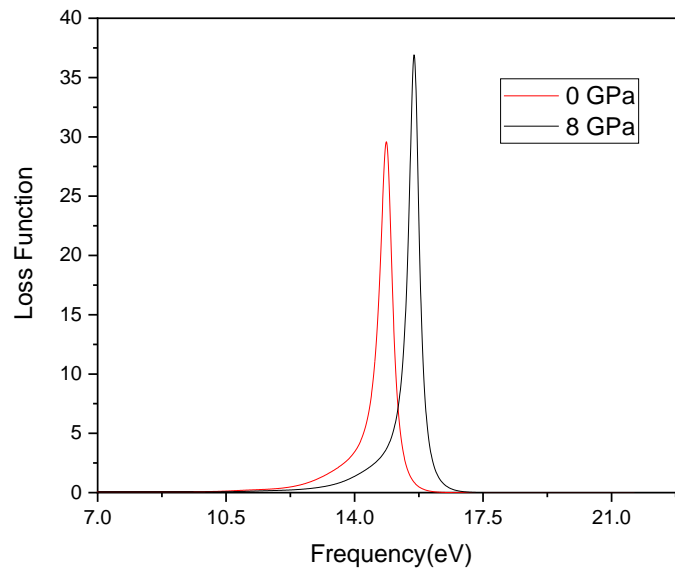

Figure III.10. Optical conductivity of the SiSn alloy at P = 0 GPa and P = 8 GPa as a function of $\hbar\omega$.

III.5.4. Electron energy lossfunction

The electron energy loss function L(ω) is a crucial parameter in analysing energy dissipation when fast electrons traverse a semiconductor. This function provides insight into the collective oscillations of electrons known as plasmon's, and their interaction with incident photons [16, 19].

We have computed the electron energy loss function L(ω) for the SiSn alloy at P = 0 GPa and P = 8 GPa using first-principles calculations. The results, displayed in **Figure III.11**, reveal a prominent plasma resonance peak at approximately $\hbar\omega_p = 14.85$ eV for P = 0 GPa, which shifts towards higher energies (~17 eV) under increased pressure. This behaviour aligns with previous findings on similar zinc-blende semiconductors [16, 24].

The pressure-induced shift in plasma frequency is attributed to the increase in electron density and the resulting modification of dielectric properties [24]. A similar trend was observed in II-VI semiconductors and other Si-based alloys, indicating that external pressure significantly affects charge carrier dynamics and optical performance [16, 24].

Figure III.11. Energy loss function of the SiSn alloy obtained at P = 0 GPa and P = 8 GPa as a function of $\hbar\omega$.
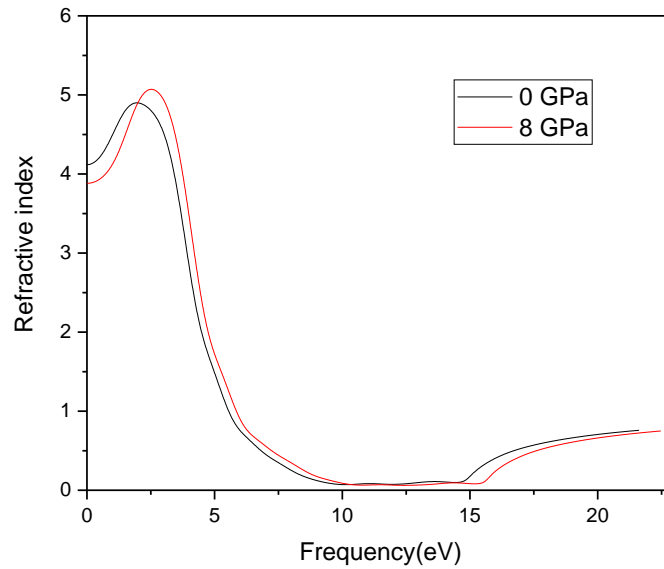
III.5.5. Refractive index

The refractive index n is a crucial physical parameter that generally depends on the wavelength of the electromagnetic wave [24]. It characterizes the behaviour of light in materials, representing their ability to slow down and bend light, thereby playing a fundamental role in optical applications [16].

The variations in the refractive index spectra n as a function of photon energy $\hbar\omega$ for the SiSn alloy at P = 0 GPa and P = 8 GPa are shown in **Figure III.12**.

At both P = 0 GPa and P = 8 GPa, the refractive index n of the SiSn alloy decreases as the photon energy increases, reaching its minimum values at $\hbar\omega \approx 10$ and 18 eV, respectively. Additionally, peaks appear in the spectra at photon energies of approximately $\hbar\omega \approx 5$ eV, which may originate from excitonic transitions occurring near the fundamental band gap Eg [19, 24].

At P = 0 GPa, the static refractive index of the SiSn alloy is estimated to be 4.8, which is slightly higher than the value of 4.6 reported for pure Si [17] and lower than 5.2 obtained for pure Sn [14]. This trend aligns with similar observations reported for other semiconductor alloys [19, 24].

Figure III.12: Refractive index n spectra of the SiSn alloy calculated for P=0 GPa and P=8 GPa as a function of $\hbar\omega$

III.5.6. Optical reflectivity

Understanding the real and imaginary components of the dielectric function is essential for calculating other optical parameters, such as the optical reflectivity spectrum under normal incidence, which is defined by the following equation [16, 19]:

$$R(\omega)=\left|\frac{\sqrt{\varepsilon(\omega)}-1}{\sqrt{\varepsilon(\omega)}+1}\right|^2 \tag{III.10}$$

where:

- $\varepsilon(\omega)$ is the complex dielectric function,

- ω is the photon energy (frequency),

- R(ω) represents the reflectivity coefficient.

The optical reflectivity spectra for the SiSn alloy at pressures of 0 GPa and 8 GPa are shown in **Figure III.13**. It is remarkable that the maximum reflectivity peak reaches approximately 75%and appears around $\hbar\omega$ = 12 eV. Applying a pressure of 8 GPa causes a slight shift of the reflectivity spectrum towards higher frequencies.

Additionally, the application of 8 GPa results in a minor change in the shape of the optical reflectivity spectrum. Moreover, it increases the maximum reflectivity peak to approximately 85%, which occurs around $\hbar\omega$ = 14.85 eV. Interestingly, this behaviour is similar to what has been observed in the binary Si and Sn compounds [24].
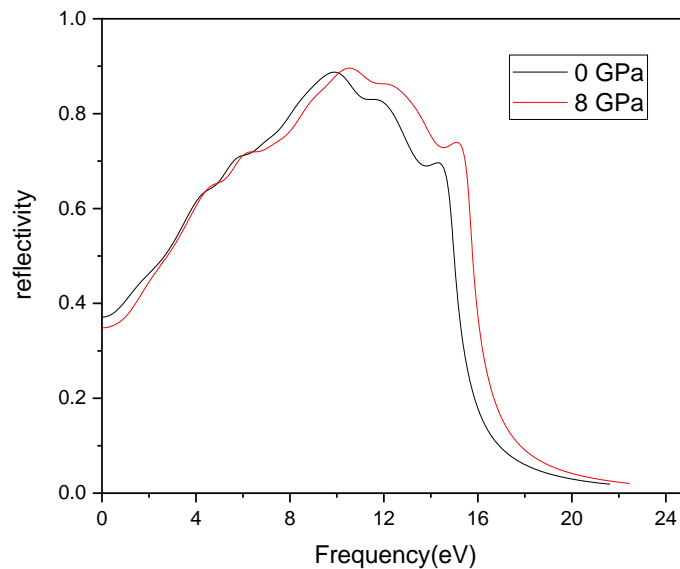
Figure III.13: Optical reflectivity spectra of the SiSn alloy calculated at P = 0 GPa and P = 8 GPa as a function of photon energy.

It is important to note that all these optical properties of the SiSn alloy were obtained using the LDA approximation, in agreement with previous studies on similar materials [24].

III.6. Conclusion

This chapter has outlined the theoretical methods used to study the SiSn alloy, highlighting the application of Density Functional Theory (DFT) and its associated computational techniques. The employment of pseudopotential methods and plane-wave expansions has been demonstrated to enhance computational efficiency while maintaining high accuracy in predicting material properties. Through structural optimisation, the equilibrium lattice

parameter is determined, while band structure calculations reveal essential electronic properties such as the band gap and charge carrier dynamics.

Moreover, the study of the optical properties of the alloy, including the dielectric function and the absorption spectra, provides further insight into the potential applications of the alloy in optoelectronic devices. Furthermore, it is important to note that external factors, such as hydrostatic pressure, have the capacity to substantially alter the electronic and optical characteristics of the SiSn alloy. This underscores the necessity for a comprehensive understanding of external perturbations within the field of material science [19, 24].

It is important to note that the use of CASTEP, a powerful DFT based computational tool, ensures the reliability and reproducibility of the simulations carried out. The knowledge gained from this theoretical framework will guide experimental studies and possible technological applications of the SiSn alloy.

The following chapter presents the numerical results obtained from the simulations, with a comprehensive analysis of the trends and implications of the results.

General Conclusion

General Conclusion

In this work, we have conducted a comprehensive theoretical investigation of the structural, electronic, and optical properties of the ordered SiSn alloy in the cubic zinc-blende phase using first-principles calculations based on Density Functional Theory (DFT). The study employed both Local Density Approximation (LDA) and Generalized Gradient Approximation (GGA) to achieve reliable and accurate predictions.

Our structural analysis confirmed the stability of the SiSn alloy, revealing optimized lattice parameters and theoretical densities consistent with the expectations for group IV semiconductors. The application of hydrostatic pressure further highlighted the alloy's mechanical response and its influence on lattice dynamics.

The electronic band structure calculations demonstrated that the SiSn alloy exhibits a semiconducting behavior with an indirect band gap, which is sensitive to pressure variations. This tunability of the band gap with pressure suggests promising applications in optoelectronic and high-performance microelectronic devices.

In addition, the optical properties including the dielectric function, absorption coefficient, conductivity, refractive index, and reflectivity were evaluated, providing insight into the material's interaction with electromagnetic radiation. These results indicate that the SiSn alloy possesses significant potential in photonic and optoelectronic technologies, especially in the infrared range.

Overall, this study contributes to the understanding of SiSn alloy behavior at the atomic scale and supports its viability for future technological applications. Future work may include the study of temperature effects, dopant incorporation, or comparison with experimental data to further validate and expand on these findings.

References

References

References

[1] A.Chellouai, Etude des propriétés structurales, électroniques, élastiques et optiques des composés à base de Scandium, Mémoire de Master, Université Med Khider Biskra, (2014).

[2] A.Khaldi, Etude des propriétés optoélectroniques et mécaniques des semiconducteurs magnétiques, Thèse de Doctorat, Université Mohamed Khider–Biskra, (2019).

[3] W. Kessal and E. Chaïb-Draa, Contribution to the study of the physical properties of the binary compound ScAs, Mémoire de Master, Université de BordjBouArreridj, (2021).

[4]A. Zaoui, M. Ferhat, M. Certier, B. Khelifa, H. Aourag, Optical properties of SiSn and GeSn,Infrared Physics & Technology, 37, 483–488 (1996). https://doi.org/10.1016/1350-4495(95)00116-6

[5]B. H. Elias, Structural, electronic, elastic, optical and thermodynamical properties of zinc-blende SiGe, SiSn and GeSn from fist principles, Advances in Physics Theories and Applications, 25 (2013) 82–91.https://www.researchgate.net/publication/302958979

[6] Java point, Difference between n-type and p-type semiconductors. https://www.javatpoint.com (Accessed: Feb. 10, 2025).

[7] S. M. Sze and K. K. Ng, *Physics of semiconductor devices*, 3rd ed., Wiley, (2006).

[8] J. Yu *et al.*, Hybrid-functional calculations of electronic structure and phase stability of MO (M = Zn, Cd, Be, Mg, Ca, Sr, Ba) and related ternary alloy $M_xZn_{1-x}O$, RSC Adv. 9 (2019) 8507–8514. https://doi.org/10.1039/C9RA00362B

[9] K. Tiwary, Classification of different types of semiconducting materials, 2020. Available: https://www.researchgate.net (Accessed: Feb. 10, 2025).
[10] D. Loss and D. P. DiVincenzo, Quantum computation with quantum dots, *Phys. Rev. A* 57 (1998)120–126. https://doi.org/10.1103/PhysRevA.57.120

[11] R. P. Feynman, "There's Plenty of Room at the Bottom," *Engineering and Science*, vol. 23, no. 5, pp. 22–36, Feb. 1960. [Online]. Available: *Caltech E-Print* repository https://resolver.caltech.edu/CaltechES:23.5.1960Bottom)

[12] H. Lee, Direct bandgap vs Indirect bandgap, *Univ Life Record,* Jun. 17, 2023.https://univ-life-record.tistory.com/entry/Direct-bandgap-vs-Indirect-bandgap.

[13] M. Abedin, Direct band-gap semiconductor and indirect band-gap semiconductor, 2016. https://www.researchgate.net/profile/MinhazAbedin (Accessed: Feb. 10, 2025).

[14] P. Hohenberg and W. Kohn, Inhomogeneous electron gas, *Phys. Rev.* B 136 (1964) 864–871. https://doi.org/10.1103/PhysRev.136.B864

[15] L. Benguedouad, T. Fadache**,** *Étude des propriétés structurales, optiques et électroniques du semi-conducteur ScP*, Mémoire de Master, Université Mohamed El-Bachir El-Ibrahimi de Bordj Bou-Arréridj, (2021)
[16] X. D. Zhang *et al.*, A first principles investigation on the structural, phonon, elastic and thermodynamic properties of the $Si_{0.5}Sn_{0.5}$ cubic alloy, *Solid State Commun.* 152 (2012) 955–959. https://doi.org/10.1016/j.ssc.2012.03.017

[17] N. Amrane, S. AitAbderrahmane, H. Aourag, Band structure calculation of GeSn and SiSn, Infrared Physics

& Technology, 36 (1995) 843–848. https://doi.org/10.1016/1350-4495(95)00019-U

[18] S. Zhao, W. Kang and J. Xue, The potential application of phosphorene as an anode material in Li-ion batteries, *J. Mater. Chem. A* 2 (2014) 19035–19040. https://www.researchgate.net/publication/378891641

[19] F. Yu *et al.*, Advances in computational material science: A review of first-principles methods and applications, Computation, 7 (4), (2019) 57.

[20] E. W. Welch, First principle modeling of hybrid halide perovskites for optoelectronic applications, PhD Dissertation, Texas State University, 2019. https://www.researchgate.net/publication/339032821

References

[21] A.Kebede, Introduction to Solid State Physics: Lecture Notes, 2015. https://www.researchgate.net/publication/281558415

[22] VASP Forum, Cut-off energy convergence discussions. https://www.vasp.at/viewtopic.php?t=10641

[23] M. D. Segall, P.J.D. Lindan, M.J. Probert, C.J. Pickard, P.J. Hasnip, S.J. Clark, M.C. Payne, First-principles simulation: ideas, illustrations and the CASTEP code, J. Phys. 14 (2002) 2717–2744. https://doi.org/10.1088/0953-8984/14/11/301

[24] X. Zhang, C. Ying, Z. Li and G. Shi, First-principles calculations of structural stability, elastic, dynamical and thermodynamic properties of SiGe, SiSn, GeSn, Superlattices Microstruct. 52 (2012) 459–469. http://dx.doi.org/10.1016/j.spmi.2012.06.001

[25] D. M. Ceperley, B. Alder, Ground state of the electron gas by a stochastic method, Phys. Rev. Lett. 45 (7), (1980) 566–569. https://doi.org/10.1103/PhysRevLett.45.566

[26] J. P. Perdew, and A. Zunger, Self-interaction correction to density-functional approximations for many-electron systems, Phys. Rev. B 23 (10) (1981) 5048–5079. https://doi.org/10.1103/PhysRevB.23.5048

[27] J. M. Gonzalez and M. A. Tome, Ab initio study of electronic, elastic and optical properties of cubic and hexagonal MgS under pressure, Physica B, 563 (2019) 131–137. doi:http://dx.doi.org/10.1016/j.physb.2018.10.018

[28] F. D. Murnaghan, *The compressibility of media under extreme pressures*, Proc. Natl. Acad. Sci. USA, 30 (1944) 244–247.https://doi.org/10.1073/pnas.30.9.244

[29] F. Birch, *Finite elastic strain of cubic crystals, Phys. Rev.*71 (1947) 809–824. https://doi.org/10.1103%2FPhysRev.71.809

[30] S. Huang, S. Ning, R. Xiong, First-principles study of silicon–tin alloys as a high-temperature thermoelectric material, *Materials*, 15 (2022) 4107. https://doi.org/10.3390/ma1512

ملخص

يتناول هذا العمل دراسة نظرية شاملة للسبيكة الثنائية SiSn المتبلورة في البنية المكعبة من نوع الزنك-بلند. تم إجراء الحسابات باستخدام نظرية الكثافة الوظيفية (DFT) باعتماد طريقة الجهد الكاذب والموجات المستوية كما هي مدمجة في كود CASTEP ، مع استخدام تقريب الكثافة المحلية (LDA) لنمذجة تأثيرات التبادل والارتباط. شملت الدراسة الخصائص البنيوية (ثابت الشبكة، معامل الانضغاط)، والخصائص الإلكترونية (بنية النطاق)، بالإضافة إلى الخصائص البصرية (معامل الانكسار، الانعكاسية، التوصيلية البصرية، معامل الامتصاص، ودالة فقد الطاقة). كما تم تحليل تأثير الضغط الهيدروستاتيكي عند 0 و8 GPa، حيث أظهرت النتائج تغيرًا ملحوظًا في فجوة الطاقة وانزياحًا في الأطياف البصرية. تؤكد هذه النتائج الإمكانات الواعدة لسبيكة SiSn في التطبيقات البصرية والإلكترونية القابلة للتحكم بالضغط. الضغط

الكلمات المفتاحية : LDA , DFT, CASTEP , شبه موصل , SiSn , الزنك-بلند , الهيدروستاتيكي

Abstract

This dissertation presents a comprehensive theoretical study of the binary SiSn alloy crystallizing in the cubic zinc-blende structure. The investigation was conducted using Density Functional Theory (DFT) combined with the pseudopotential and plane-wave approach, as implemented in the CASTEP code. The Local Density Approximation (LDA) was employed to model exchange-correlation effects. The study encompasses structural (lattice constant, bulk modulus), electronic (band structure), and optical (refractive index, reflectivity, optical conductivity, absorption coefficient, and energy loss function) properties. The effect of hydrostatic pressure (0 and 8 GPa) was also examined, revealing significant band gap modulation and spectral shifts. The findings underscore the potential of SiSn as a pressure-tunable material for next-generation optoelectronic applications.

Keywords: CASTEP, DFT, LDA, semiconductor, SiSn, zinc-blende, hydrostatic pressure.

Résumé

Ce mémoire présente une étude théorique approfondie de l'alliage binaire SiSn, cristallisé dans la phase cubique de type zinc-blende. Les propriétés structurales, électroniques et optiques de cet alliage ont été étudiées à l'aide de la théorie de la fonctionnelle de la densité (DFT), en utilisant l'approche des pseudopotentiels avec ondes planes telle qu'implémentée dans le code CASTEP. L'approximation de la densité locale (LDA) a été adoptée pour traiter les effets d'échange-corrélation. Les calculs ont permis de déterminer le paramètre de maille, le module de compressibilité, la structure de bande, ainsi que des propriétés optiques telles que l'indice de réfraction, la réflectivité, la conductivité optique, la fonction de perte d'énergie et le coefficient d'absorption. L'influence de la pression hydrostatique (0 et 8 GPa) a également été explorée, montrant une modification notable du gap électronique et un décalage des spectres optiques. Ces résultats mettent en évidence le potentiel de l'alliage SiSn pour des applications optoélectroniques sensibles à la pression.

Mots-clés : CASTEP, DFT, LDA, semiconducteur, SiSn, zinc-blende, pression hydrosta